Hindawi
Mathematical Problems in Engineering
Volume 2019, Article ID 5791579, 15 pages
https://doi.org/10.1155/2019/5791579

Research Article

Extended-State-Observer-Based Terminal Sliding Mode Tracking Control for Synchronous Fly-Around with Space Tumbling Target

Zhijun Chen,[1] Yong Zhao,[1] Yuzhu Bai,[1] Dechao Ran,[2] and Liang He[1]

[1]*College of Aerospace Science and Engineering, National University of Defense Technology, Changsha 410073, China*
[2]*National Innovation Institute of Defense Technology, Chinese Academy of Military Science, Beijing 100091, China*

Correspondence should be addressed to Yong Zhao; zhaoyong@nudt.edu.cn

Received 23 June 2019; Revised 4 August 2019; Accepted 11 August 2019; Published 5 November 2019

Academic Editor: Alberto Cavallo

This paper presents a robust controller with an extended state observer to solve the Synchronous Fly-Around problem of a chaser spacecraft approaching a tumbling target in the presence of unknown uncertainty and bounded external disturbance. The rotational motion and time-varying docking trajectory of tumbling target are given in advance and referred as the desired tracking objective. Based on dual quaternion framework, a six-degree-of-freedom coupled relative motion between two spacecrafts is modeled, in which the coupling effect, model uncertainties, and external disturbances are considered. More specially, a novel nonsingular terminal sliding mode is designed to ensure the convergence to the desired trajectory in finite time. Based on the second-order sliding mode, an extended state observer is employed to the controller to compensate the closed-loop system. By theoretical analysis, it is proved that the modified extended-state-observer-based controller guarantees the finite-time stabilization. Numerical simulations are taken to show the effectiveness and superiority of the proposed control scheme. Finally, Synchronous Fly-Around maneuvers can be accomplished with fast response and high accuracy.

1. Introduction

Synchronous Fly-Around (SFA) technique represents the concept of proximity operation for driving a chaser spacecraft to fly around a space tumbling target with attitude synchronized. With the number of failed spacecraft and space debris increasing, on-orbit service operations are urgently required to extend life of the failed spacecrafts, such as assembly, repairing, module replacement, detumbling, refueling, and orbital debris removal [1, 2]. Under the influence of terrestrial gravitational perturbation, most of the failed spacecrafts have evolved into space tumbling targets, developing the noncooperative feature [3]. The SFA approach (see Figure 1) can be identified as a significant technology for on-orbit service missions since it performs high accuracy in close-range proximity to noncooperative tumbling target. Some studies have been performed with the intention to solve the SFA problem [4–7].

As pointed out in [8], it also introduces a series of problems and challenges in SFA process. Different from traditional cooperative space missions, rendezvous and docking (RVD), and spacecraft formation flying (SFF), the noncooperative characteristics of SFA will result in deficiency of shape structure and quality information, which causes low accuracy of navigation in close proximity. Another problem is complicated modeling. It is obvious that SFA is a six-degree-of-freedom (6-DOF) relative motion, in which both the translational motion and rotational one are included. Mutual coupling between the two motions will also lead to complexity in modeling. Therefore, high precise modeling is an essential step to overcome the highly coupled drawback during SFA mission. Ma et al. [9] used C-W dynamics equation to establish the relative translational motion and adopted modified Rodrigues parameters to describe the relative rotational dynamics. Similar modeling method has also been performed in [10]. More recently, Xu et al. [11] considered the dynamical coupling inside the 6-DOF model and presented a nonlinear suboptimal control law for SFA problem. However, all the abovementioned studies gave the two-part relative motion and ignored the nonlinear coupling effect [12], such that it would cause the problem that rotational and translational control will not

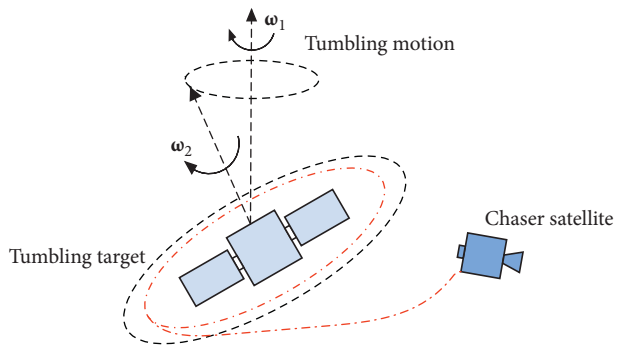

Figure 1: Synchronous fly-around for a chaser approaching a tumbling target.

actuate simultaneously. Therefore, it is significant to establish integrated 6-DOF relative motion considering coupled term. Dual quaternion [13–15] gives us inspiration to solve SFA problem since it has been an effective tool for motion description in physical problems and mathematical calculation. It combines traditional Euler quaternions with dual numbers and inherits elegant properties of both. Based on dual quaternion, the coupled 6-DOF dynamics motion between two spacecrafts can be derived successfully. Wang et al. [12] made attempt to use dual quaternion to describe the coupled dynamics of rigid spacecraft and investigated the coordinated control problem for SFF problem. Wu et al. [16, 17] proposed a nonlinear suboptimal control based on dual quaternion for synchronized attitude-position control problem. Under dual-quaternion framework, Filipe and Tsiotras [18] proposed an adaptive tracking controller for spacecraft formation problem and ensured global asymptotical stability in the presence of unknown disturbance. For the safety problem of RVD, Dong et al. [19] proposed a dual-quaternion-based artificial potential function (APF) control to guarantee the arrival at the docking port of the target with desired attitude. The above research results illustrate the effectiveness of 6-DOF modeling using dual-quaternion framework and also provide the motivation of this paper.

The guidance, navigation, and control (GNC) systems for space proximity operations should be taken into account during on-orbit SFA missions [20]. Due to the nonlinear and highly coupled dynamics, designing a controller for the accurate SFA operation is still an open problem. In addition to the preceding interests in 6-DOF modeling, uncertainties and disturbances are another key issue that should be addressed in the control system, which will severely reduce the performance of the controller or lead to instability of the closed-loop system. Therefore, it is urgent to realize accurate and fast SFA tracking control, under strong coupling effects and multisource interferences in practical process. In view of this problem, various nonlinear control methods have been carried out to estimate the disturbance and compensate the system, such as state-dependent Riccati equation (SDRE) control [21], adaptive control [22] and suboptimal control [11]. Among these methods, terminal sliding mode (TSM) control is an effective technique due to its robustness to system uncertainties and can provide finite-time convergence. Wang and Sun [23] carried out an adaptive TSM control method for spacecraft formation flying problem within dual-quaternion framework. However, the major disadvantage of initial TSM is the singularity problem. In order to eliminate this problem, Zou et al. [24] proposed a nonsingular TSM control (NTSMC) to realize the finite-time stability of satellite attitude control. Extended-state-observer (ESO) methods have recently been introduced to compensate for unmodeled dynamics and system with external disturbance and uncertainty. Conventional ESO has shown fine performance in disturbance rejection. Based on a new technique known as the second-order sliding mode (SOSM) [25], a novel ESO can guarantee high accuracy and robustness of the estimation with finite-time convergence. Some studies have recently combined conventional TSM and ESO for spacecraft control problem [26, 27]. Moreover, the combination of NTSMC and ESO is also widely used, especially in aerospace engineering, such as attitude tracking control [28, 29], underactuated spacecraft hovering [30], and reusable launch vehicle [31]. In Reference [28], an ESO-based third-order NTSMC was proposed for the attitude tracking control problem. Ran et al. [32] proposed an adaptive SOSM-based ESO with fault-tolerant NTSMC for the model uncertainty, external disturbance, and limited actuator control during spacecraft attitude control. Zhang et al. [33] presented an adaptive fast NTSMC using estimated information by SOSM-based ESO to solve the problem of spacecraft 6-DOF coupled tracking maneuver in the presence of model uncertainties and actuator misalignment. Moreno and Osori [25] gave a Lyapunov finite-time stability proof for a closed-loop system combining SOSM controller and ESO. To the best of the authors' knowledge, ESO-based NTSMC is still an open problem for SFA mission within dual-quaternion framework.

This paper aims to investigate the Synchronous Fly-Around maneuver problem in the presence of model uncertainties and external disturbances. Compared to existing results, the major contributions and differences of this study are summarized as follows:

(1) To date, it is the first time to use dual quaternion to describe 6-DOF relative dynamics for tumbling target-capturing problem, in which the nonlinear coupled effect, model uncertainties, and external disturbances are taken into account. Moreover, the error kinematics and dynamics are given to improve modeling accuracy significantly.

(2) Motivated by the concept of SOSM, a novel ESO is proposed to reconstruct the model uncertainties and external disturbances with finite-time convergence. Based on the estimated information of ESO, a fast NTSMC is carried out to eliminate the total disturbances and ensure the finite-time stable of the closed-loop system. The proposed method can gain faster response and higher accuracy than existing methods.

This paper is organized as follows. Some necessary mathematical preliminaries of dual quaternion and useful lemmas are given and coupled kinematics and dynamics are derived for the relative motion problem in Section 2. In

Section 3, NTSMC and ESO strategies are elaborated, and the finite-time stability analysis of the system is performed in Section 4. Following that, numerical simulations are illustrated and discussed in Section 5 to show the effectiveness of the proposed method. Finally, some appropriate conclusions are presented in Section 6.

2. Mathematical Preliminaries

This study considers the leader-follower spacecraft formation, including a chaser and a tumbling target (Figure 2). In order to facilitate the description of the model, the following coordinate system is used: $O_I - X_I Y_I Z_I$ is the Earth-centered inertial coordinate system, with the Cartesian right-hand reference frame; $O_l - x_l y_l z_l$ is LVLH (local-vertical, local-horizontal) reference frame with the origin at the center of mass of target, x_l is pointing to the spacecraft radially outward; z_l is the axis normal to the target orbital plane, and y_l is the axis established by right-hand rule; $O_f - x_f y_f z_f$ (respectively, the tumbling target, $O_l - x_l y_l z_l$) is the body-fixed coordinate system of the chaser, with its origin in the center of mass of the chaser and axes pointing to the axis of inertial; $P_l - x_l y_l z_l$ is the desired tracking reference frame, with the capturing point P_l of the tumbling target. The control objective is to control the chaser ($O_f - x_f y_f z_f$) synchronize with desired state ($P_l - x_l y_l z_l$) so that the on-orbit service can be guaranteed in the next step.

2.1. Dual Quaternion. Dual quaternion can be regarded as a quaternion whose element is dual numbers and can be defined as [14, 15, 23].

$$\hat{q} = [\hat{\eta}, \hat{\xi}] = q + \varepsilon q', \tag{1}$$

where $\hat{\eta}$ is the dual scalar part; $\hat{\xi} = [\hat{\xi}_1, \hat{\xi}_2, \hat{\xi}_3]$ is the dual vector part; q and q' are the traditional Euler quaternions, representing the real part and dual part of dual quaternion, respectively; and ε is the called dual unit with $\varepsilon^2 = 0$ and $\varepsilon \neq 0$. In this paper, $\mathbb{N}$ is employed to denote the set of dual quaternions and $\mathbb{R}$ denotes the set of dual numbers. Therefore, it is supposed that $\hat{q} \in \mathbb{N}^4$, $\hat{\xi} \in \mathbb{R}^3$, and $\hat{\eta} \in \mathbb{R}$.

Similar to the traditional quaternion and dual vector (see Appendix), the basic operations for dual quaternions are given as follows:

$$\begin{aligned} \hat{q}_1 + \hat{q}_2 &= \left[\hat{\eta}_1 + \hat{\eta}_2, \hat{\xi}_1 + \hat{\xi}_2\right], \\ \lambda\hat{q} &= [\lambda\hat{\eta}, \lambda\hat{\xi}], \\ \hat{q}^* &= [\hat{\eta}, -\hat{\xi}], \\ \hat{q}_1 \otimes \hat{q}_2 &= \left[\hat{\eta}_1\hat{\eta}_2 - \hat{\xi}_1\hat{\xi}_2, \hat{\eta}_1\hat{\xi}_2 + \hat{\eta}_2\hat{\xi}_1 + \hat{\xi}_1 \times \hat{\xi}_2\right], \end{aligned} \tag{2}$$

where $\hat{q}_1 = [\hat{\eta}_1, \hat{\xi}_1]$ and $\hat{q}_2 = [\hat{\eta}_2, \hat{\xi}_2]$, λ is a scalar, and $\hat{q}^*$ represents the conjugate of $\hat{q}$.

Using dual quaternion, the frame $O_f - x_f y_f z_f$ with respect to frame $O_l - x_l y_l z_l$ can be defined as

$$\hat{q}_{fl} = \hat{q}_l^* \otimes \hat{q}_f = q_{fl} + \varepsilon\frac{1}{2}\mathbf{p}_{fl}^l \otimes q_{fl} = q_{fl} + \varepsilon\frac{1}{2}q_{fl} \otimes \mathbf{p}_{fl}^f, \tag{3}$$

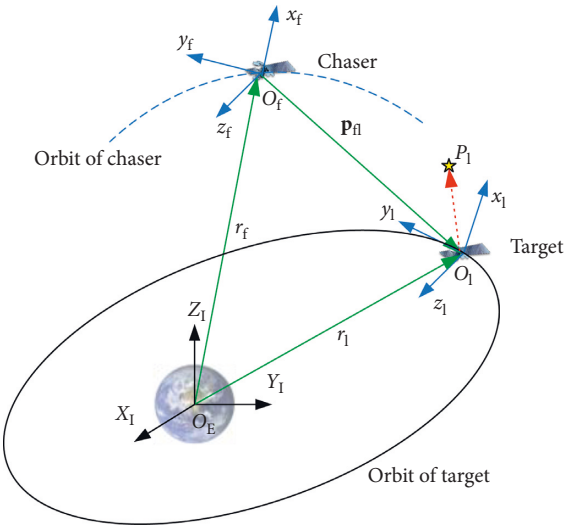

Figure 2: Coordinate system definition.

where $\hat{q}_l$ and $\hat{q}_f$ represent the dual quaternion of frame of the target and the chaser, respectively; q_{fl} is the relative quaternion; $\mathbf{p}_{fl}^l$ and $\mathbf{p}_{fl}^f$ are the relative position vectors of the chaser relative to the target, expressed in frames $O_l - x_l y_l z_l$ and $O_f - x_f y_f z_f$, respectively.

2.2. Relative Kinetics and Coupled Dynamics. Referring to [12, 18, 23], the kinematics and coupled dynamics equation of $O_l - x_l y_l z_l$ with respect to $O_f - x_f y_f z_f$ using dual quaternion representation can be described as follows:

$$\begin{aligned} 2\dot{\hat{q}}_{fl} &= \hat{q}_{fl} \otimes \hat{\omega}_{fl}^f, \\ \dot{\hat{\omega}}_{fl}^f &= -\hat{\mathbf{M}}_f^{-1}\left[\left(\hat{\omega}_{fl}^f + \hat{q}_{fl}^* \otimes \hat{\omega}_l^l \otimes \hat{q}_{fl}\right) \times \hat{\mathbf{M}}_f\left(\hat{\omega}_{fl}^f + \hat{q}_{fl}^* \otimes \hat{\omega}_l^l \otimes \hat{q}_{fl}\right)\right] \\ &\quad + \hat{\mathbf{M}}_f^{-1}\hat{F}_f^f - \hat{q}_{fl}^* \otimes \dot{\hat{\omega}}_l^l \otimes \hat{q}_{fl} + \hat{\omega}_{fl}^f \times \left(\hat{q}_{fl}^* \otimes \hat{\omega}_l^l \otimes \hat{q}_{fl}\right), \end{aligned} \tag{4}$$

where $\hat{\omega}_{fl}^f = \omega_{fl}^f + \varepsilon(\dot{p}_{fl}^f + \omega_{fl}^f \times \mathbf{p}_{fl}^f) \in \mathbb{N}^3$ is the relative velocity-expressed frame $O_f - x_f y_f z_f$; ω_{fl}^f is the relative angular velocity; and $\dot{p}_{fl}^f$ is the relative linear velocity between two frames. As can be seen from the definition, $\hat{\omega}_{fl}^f$ can also be written as $\hat{\omega}_{fl}^f = \hat{\omega}_f^f - \hat{q}_{fl}^* \otimes \hat{\omega}_l^l \otimes \hat{q}_{fl}$. Besides, the force $\hat{F}_f^f = \hat{F}_u^f + \hat{F}_g^f + \hat{F}_d^f$ is the total dual force; $\hat{F}_g^f = f_g^f + \varepsilon\tau_g^f$ is the dual gravity; $\hat{F}_u^f = f_u^f + \varepsilon\tau_u^f$ is the dual control force; $\hat{F}_d^f = f_d^f + \varepsilon\tau_d^f$ is the dual disturbance; and f_g^f is the dual gravity force and τ_g^f is the dual gravity torque referred to the chaser ($\hat{F}_u^f = f_u^f + \varepsilon\tau_u^f$ and $\hat{F}_d^f = f_d^f + \varepsilon\tau_d^f$, respectively). $\hat{\mathbf{M}}_f = m_f(d/d\varepsilon)\mathbf{I} + \varepsilon J_f$ is the dual inertia matrix of chaser, in which m_f and J_f are the mass and moment of inertia of chaser.

2.3. Lemmas. The lemmas useful for this study are introduced as follows. Firstly, the following system is considered:

$$\begin{aligned} \dot{x} &= f(x, u, t), \\ f(0, t) &= 0, \end{aligned} \tag{5}$$

where $x \in R^n$ is the system status and $u \in R^m$ is the control input.

Lemma 1 (see [34]). *Suppose Φ is a positive definite function and there exists scalar $\upsilon > 0$, $0 < \alpha < 1$, and satisfies*

$$\dot{\Phi}(x) + \upsilon\Phi^{\alpha}(x) \le 0, \quad x \in U_0, \tag{6}$$

then there is an field $U_0 \subset R^n$ so that the $\Phi(x)$ can reach equilibrium point in finite time. And the convergence time is satisfied as

$$T_1 \le \frac{\Phi_0^{1-\alpha}}{\upsilon - \upsilon\alpha}. \tag{7}$$

Lemma 2 (see [35]). *Suppose Θ is a positive definite function and there are scalars $\rho_1 > 0$ and $\rho_2 > 0$, $0 < \beta < 1$, and satisfies*

$$\dot{\Theta}(x) \le -\rho_1\Theta(x) - \rho_2\Theta^{\beta}(x), \quad x \in U_1, \tag{8}$$

then there is a field $U_1 \subset R^n$ so that the $\Theta(x)$ can reach equilibrium point in finite time. And the convergence time is satisfied as

$$T_2 \le \frac{1}{\rho_1(1-\beta)} \ln \frac{\rho_1\Theta_0^{1-\beta} + \rho_2}{\rho_2}. \tag{9}$$

2.4. Problem Formulation. The control objective of this paper is to design a controller so that the relative motion state $[\widehat{q}_{\mathrm{fl}}(t), \widehat{\boldsymbol{\omega}}_{\mathrm{fl}}^{\mathrm{f}}(t)]$ of the chaser converges to the desired state $[\widehat{q}_{\mathrm{d}}(t), \widehat{\boldsymbol{\omega}}_{\mathrm{d}}(t)]$ in finite time. In order to describe the relative motion between the chaser and the capturing point of tumbling target, the relative motion between the reference frame $P_{\mathrm{l}} - x_{\mathrm{l}}y_{\mathrm{l}}z_{\mathrm{l}}$ and frame $O_{\mathrm{f}} - x_{\mathrm{f}}y_{\mathrm{f}}z_{\mathrm{f}}$ is established. Firstly, the description of target's attitude is given which is considered as the general Euler attitude motion. The kinematics and dynamic are shown as follows, respectively:

$$\begin{aligned} 2\dot{q}_{\mathrm{l}} &= q_{\mathrm{l}} \circ \boldsymbol{\omega}_{\mathrm{l}}^{\mathrm{l}}, \\ J_{\mathrm{l}}\dot{\omega}_{\mathrm{l}}^{\mathrm{l}} &= -\boldsymbol{\omega}_{\mathrm{l}}^{\mathrm{l}} \times J_{\mathrm{l}}\boldsymbol{\omega}_{\mathrm{l}}^{\mathrm{l}} + \tau_{\mathrm{d}}, \end{aligned} \tag{10}$$

where q_{l} is the quaternion of the tumbling target; $\boldsymbol{\omega}_{\mathrm{l}}^{\mathrm{l}}$ is the angular velocity expressed in $O_{\mathrm{l}} - x_{\mathrm{l}}y_{\mathrm{l}}z_{\mathrm{l}}$; J_{l} is the moment of inertia of tumbling target; and τ_{d} is the total disturbance torque acting on target. The operation $\circ$ represents the multiplication of traditional quaternion.

The position vector of reference point P_{l} with respect to the centroid O_{l} on the tumbling target in the frame $O_{\mathrm{f}} - x_{\mathrm{f}}y_{\mathrm{f}}z_{\mathrm{f}}$ is represented as follows:

$$\mathbf{p}_{\mathrm{fl}}^{\mathrm{f}} = q_{\mathrm{fl}}^{*} \circ P_{\mathrm{l}} \circ q_{\mathrm{fl}}, \tag{11}$$

where q_{fl} is the attitude quaternion of the chaser relative to the target and P_{l} is the position of the noncentroid point P_{l} with respect to the centroid O_{l} at the initial moment.

Remark 1. Referring to [36], some information of relative motion can be measured. The model of 3D reconstruction which is obtained by the mathematical alignment of the image plane and binocular stereo matching is established to determine the relative position and pose of the target's capturing point. In such a way, relative rotational and translational motion between two spacecrafts can be obtained.

Considering the external disturbances and model uncertainty of the spacecraft, the error kinematics and dynamics equations based on $\widehat{q}_{\mathrm{e}}$ and $\widehat{\boldsymbol{\omega}}_{\mathrm{e}}$ can be obtained as

$$\begin{aligned} 2\dot{\widehat{q}}_{\mathrm{e}} &= \widehat{q}_{\mathrm{e}} \otimes \widehat{\boldsymbol{\omega}}_{\mathrm{e}}, \\ \widehat{\mathbf{M}}_0\dot{\widehat{\boldsymbol{\omega}}}_{\mathrm{e}} &= -\left(\widehat{\boldsymbol{\omega}}_{\mathrm{e}} + \widehat{q}_{\mathrm{e}}^{*} \otimes \widehat{\boldsymbol{\omega}}_{\mathrm{d}} \otimes \widehat{q}_{\mathrm{e}}\right) \times \widehat{\mathbf{M}}_0\left(\widehat{\boldsymbol{\omega}}_{\mathrm{e}} + \widehat{q}_{\mathrm{e}}^{*} \otimes \widehat{\boldsymbol{\omega}}_{\mathrm{d}} \otimes \widehat{q}_{\mathrm{e}}\right) \\ &\quad - \widehat{\mathbf{M}}_0\left(\widehat{q}_{\mathrm{e}}^{*} \otimes \dot{\widehat{\boldsymbol{\omega}}}_{\mathrm{d}} \otimes \widehat{q}_{\mathrm{e}}\right) + \widehat{\mathbf{M}}_0\widehat{\boldsymbol{\omega}}_{\mathrm{e}} \times \left(\widehat{q}_{\mathrm{e}}^{*} \otimes \widehat{\boldsymbol{\omega}}_{\mathrm{d}} \otimes \widehat{q}_{\mathrm{e}}\right) \\ &\quad + \widehat{F}_u + \widehat{F}_{g0} + \widehat{F}_{\mathrm{d}} + \Delta\widehat{F}_g + \Delta\widehat{\Sigma}, \end{aligned} \tag{12}$$

where $\widehat{\boldsymbol{\omega}}_{\mathrm{e}} = \widehat{\boldsymbol{\omega}}_{\mathrm{fl}}^{\mathrm{f}} - \widehat{q}_{\mathrm{e}}^{*} \otimes \widehat{\boldsymbol{\omega}}_{\mathrm{d}} \otimes \widehat{q}_{\mathrm{e}} = \boldsymbol{\omega}_{\mathrm{e}} + \varepsilon\nu_{\mathrm{e}}$ and $\widehat{q}_{\mathrm{e}} = \widehat{q}_{\mathrm{d}}^{-1} \otimes \widehat{q}_{\mathrm{fl}} = q_{\mathrm{e}} + \varepsilon\mathbf{p}_{\mathrm{e}}$ are the dual tracking error; q_{e} and p_{e} are the rotation error and translation error, respectively; $\boldsymbol{\omega}_{\mathrm{e}}$ and ν_{e} are the angular velocity error and linear velocity error, respectively; $\widehat{\mathbf{M}}_0$ and $\Delta\widehat{\mathbf{M}}$ are the nominal and uncertain parts of the dual matrix inertia matrix; $\widehat{F}_{\mathrm{d}}$ is the bounded disturbance; $\widehat{F}_{\mathrm{g0}}$ and $\Delta\widehat{F}_{\mathrm{g}}$ are the dual gravity associated with $\widehat{\mathbf{M}}_0$ and $\Delta\widehat{\mathbf{M}}$; and $\Delta\widehat{\Sigma}$ is the uncertainty of the dual inertia matrix and the value of which is

$$\begin{aligned} \Delta\widehat{\Sigma} &= -\widehat{\mathbf{M}}_0\dot{\widehat{\boldsymbol{\omega}}}_{\mathrm{e}} - \left(\widehat{\boldsymbol{\omega}}_{\mathrm{e}} + \widehat{q}_{\mathrm{e}}^{*} \otimes \widehat{\boldsymbol{\omega}}_{\mathrm{d}} \otimes \widehat{q}_{\mathrm{e}}\right) \times \Delta\widehat{\mathbf{M}}\left(\widehat{\boldsymbol{\omega}}_{\mathrm{e}} + \widehat{q}_{\mathrm{e}}^{*} \otimes \widehat{\boldsymbol{\omega}}_{\mathrm{d}} \otimes \widehat{q}_{\mathrm{e}}\right) \\ &\quad - \Delta\widehat{\mathbf{M}}\left(\widehat{q}_{\mathrm{e}}^{*} \otimes \dot{\widehat{\boldsymbol{\omega}}}_{\mathrm{d}} \otimes \widehat{q}_{\mathrm{e}}\right) + \Delta\widehat{\mathbf{M}}\widehat{\boldsymbol{\omega}}_{\mathrm{e}} \times \left(\widehat{q}_{\mathrm{e}}^{*} \otimes \widehat{\boldsymbol{\omega}}_{\mathrm{d}} \otimes \widehat{q}_{\mathrm{e}}\right). \end{aligned} \tag{13}$$

3. Controller Design

This section mainly studies the control problem, and modified controller of ESO-NTSMC is given. By defining the dual quaternion tracking error as $\widehat{\boldsymbol{\Omega}}_{\mathrm{e}} = \boldsymbol{\Omega}_{\mathrm{e}} + \varepsilon p_{\mathrm{e}}$ with $\boldsymbol{\Omega}_{\mathrm{e}} = 2\ln(q_{\mathrm{e}})$, the controller is designed to make the tracking error $(\widehat{\boldsymbol{\Omega}}_{\mathrm{e}}, \widehat{\boldsymbol{\omega}}_{\mathrm{e}})$ converge to $(\widehat{0}, \widehat{0})$ in finite time.

3.1. Nonsingular Terminal Sliding Mode Controller Design. In order to achieve the control objective, a fast terminal sliding surface is defined as

$$s = \dot{x} + \alpha_1 x + \alpha_2 x^{p}, \tag{14}$$

where $x \in R$ and p is a constant which satisfies $0.5 < p < 1$ and α_1 and α_2 are both positive normal numbers. The time derivative of the sliding surface s is

$$\dot{s} = \ddot{x} + \alpha_1\dot{x} + p\alpha_2 x^{p-1}\dot{x}. \tag{15}$$

As can be seen, when $x = 0$, $\dot{x} \neq 0$, and $p - 1 < 0$, the singularity may occur in equation (15). Motivated by [24, 37], an alternative form of sliding surface is proposed as follows to avoid singularity:

$$s = \dot{x} + \alpha_1 x + \alpha_2\beta(x), \tag{16}$$

where $\beta(x)$ is

$$\beta(x) = \begin{cases} \operatorname{sgn}(x)|x|^{p}, \text{if } \bar{s} = 0 \text{ or } \bar{s} \neq 0, & |x| \geq \mu, \\ \gamma_1 x + \gamma_2 \operatorname{sgn}(x) x^2, \text{if } \bar{s} \neq 0, & |x| \leq \mu. \end{cases} \tag{17}$$

In the above formula, $\gamma_1 = (2-p)\mu^{p-1}$ and $\gamma_2 = (p-1)\mu^{p-2}$ are the parameters; $\bar{s} = \dot{x} + \alpha_1 x + \alpha_2 \operatorname{sgn}(x)|x|^p$ is the nominal sliding surface; and μ is a positive small constant. Therefore, the time derivative of sliding surface (16) is

$$\dot{s} = \begin{cases} \ddot{x} + \alpha_1 \dot{x} + p\alpha_2 \operatorname{sgn}(x)|x|^{p-1}\dot{x}, \text{if } \bar{s} = 0 \text{ or } \bar{s} \neq 0, & |x| \geq \mu, \\ \ddot{x} + \alpha_1 \dot{x} + \alpha_2 \left(\gamma_1 \dot{x} + 2\gamma_2 \operatorname{sgn}(x) x \dot{x}\right), \text{if } \bar{s} \neq 0, & |x| \leq \mu. \end{cases} \tag{18}$$

Remark 2. The conventional nonsingular sliding mode (NTSM) in Reference [38]was proposed as

$$s = x + \xi \dot{x}^{m/n}, \tag{19}$$

where $x \in R$; $\xi > 0$; and q and p are the positive odd integers satisfying $1 < (m/n) < 2$. In Reference [39], it has been proved that the NTSM (19) is still singular when a dual sliding mode surface control method is designed. Furthermore, as explained in Reference [24], the NTSM (19) has slower convergence rate than the linear sliding mode when the sliding mode $s = 0$ is reached. Therefore, in order to overcome this disadvantage, the fast NTSM is proposed in this paper. The singularity of TSM is avoided by switching from terminal to general sliding manifold, which is function $\gamma_1 x + \gamma_2 \operatorname{sgn}(x) x^2$ in equation (17).

Equation (18) is continuous, and singularity is avoided. According to above derivation, the paper propose a fast NTSM surface as

$$\hat{s} = \hat{\boldsymbol{\omega}}_{\mathrm{e}} + \hat{\beta} \odot \hat{\boldsymbol{\Omega}}_{\mathrm{e}} + \hat{c} \odot \chi\left(\hat{\boldsymbol{\Omega}}_{\mathrm{e}}\right), \tag{20}$$

where $\hat{\beta} = \beta + \varepsilon\beta' \in \mathbb{R}^3$ is the positive dual constant, with $\beta > 0$ and $\beta' > 0$, so does $\hat{c} = c + \varepsilon c' \in \mathbb{R}^3$; the operation of $\odot$ is defined in Appendix; $\chi(\hat{\boldsymbol{\Omega}}_{\mathrm{e}}) = [\chi(\hat{\boldsymbol{\Omega}}_{\mathrm{e}1}), \chi(\hat{\boldsymbol{\Omega}}_{\mathrm{e}2}), \chi(\hat{\boldsymbol{\Omega}}_{\mathrm{e}3})]^{\mathrm{T}}$ is designed as follows:

$$\chi\left(\hat{\boldsymbol{\Omega}}_{ei}\right) = \begin{cases} \operatorname{sig}^{\alpha}\left(\hat{\boldsymbol{\Omega}}_{ei}\right), \text{if } \bar{\hat{s}} = 0 \text{ or } \bar{\hat{s}} \neq 0, & \left|\hat{\boldsymbol{\Omega}}_{ei}\right| \geq \varepsilon_0, \\ \gamma_1 \hat{\boldsymbol{\Omega}}_{ei} + \gamma_2 \operatorname{sgn}\left(\hat{\boldsymbol{\Omega}}_{ei}\right)\left|\hat{\boldsymbol{\Omega}}_{ei}\right|^2, \text{if } \bar{\hat{s}} \neq 0, & \left|\hat{\boldsymbol{\Omega}}_{ei}\right| \leq \varepsilon_0, \\ & i = 1, 2, 3, \end{cases} \tag{21}$$

where $\operatorname{sig}^{\alpha}(\hat{\boldsymbol{\Omega}}_{ei}) = \operatorname{sgn}(\boldsymbol{\Omega}_{ei})|\boldsymbol{\Omega}_{ei}|^{\alpha} + \varepsilon \operatorname{sgn}(\mathbf{p}_{ei})|\mathbf{p}_{ei}|^{\alpha}$; $(1/2) < \alpha < 1$; ε_0 is a positive value; $\gamma_1 = (2-\alpha)\mu^{\alpha-1}$ and $\gamma_2 = (\alpha-1)\mu^{\alpha-2}$; and $\bar{\hat{s}} = \hat{\boldsymbol{\omega}}_{\mathrm{e}} + \hat{\beta} \odot \hat{\boldsymbol{\Omega}}_{\mathrm{e}} + \hat{c} \odot \operatorname{sig}^{\alpha}(\hat{\boldsymbol{\Omega}}_{\mathrm{e}})$.

Taking derivation of the sliding surface $\hat{s}$ with respect to time yields

$$\dot{\hat{s}} = \dot{\hat{\boldsymbol{\omega}}}_{\mathrm{e}} + \hat{\beta} \odot \dot{\hat{\boldsymbol{\Omega}}}_{\mathrm{e}} + \hat{c} \odot \dot{\chi}\left(\hat{\boldsymbol{\Omega}}_{\mathrm{e}}\right), \tag{22}$$

where $\dot{\chi}(\hat{\boldsymbol{\Omega}}_{ei})$ is

$$\dot{\chi}\left(\hat{\boldsymbol{\Omega}}_{ei}\right) = \begin{cases} \alpha\left|\hat{\boldsymbol{\Omega}}_{\mathrm{e}}\right|^{\alpha-1}\dot{\hat{\boldsymbol{\Omega}}}_{\mathrm{e}}, \text{if } \bar{\hat{s}} = 0 \text{ or } \bar{\hat{s}} \neq 0, & \left|\hat{\boldsymbol{\Omega}}_{ei}\right| \geq \varepsilon_0, \\ \gamma_1 \dot{\hat{\boldsymbol{\Omega}}}_{ei} + 2\gamma_2 \operatorname{sgn}\left(\hat{\boldsymbol{\Omega}}_{ei}\right)\left|\hat{\boldsymbol{\Omega}}_{ei}\right|\dot{\hat{\boldsymbol{\Omega}}}_{ei}, \text{if } \bar{\hat{s}} \neq 0, & \left|\hat{\boldsymbol{\Omega}}_{ei}\right| \leq \varepsilon_0, \\ & i = 1, 2, 3. \end{cases} \tag{23}$$

The NTSMC method is

$$\hat{F}_u^{\mathrm{f}} = \hat{F}_{\mathrm{e}} + \hat{F}_s, \tag{24}$$

where $\hat{F}_s = -\hat{k} \odot \operatorname{sig}^{p_1}(\hat{s})$ is the switching term, $\hat{k} \in \mathbb{R}^3$ with $\hat{k}_i = k_i + \varepsilon k_i'$, $i = 1, 2, 3$, satisfying $k_i > 0$ and $k_i' > 0$; $p_1 > 0$; and $\hat{F}_{\mathrm{e}}$ is the equivalent term and the value of which is

$$\begin{aligned} \hat{F}_{\mathrm{e}} = {} & \left(\hat{\boldsymbol{\omega}}_{\mathrm{e}} + \hat{q}_{\mathrm{e}}^{*} \otimes \hat{\boldsymbol{\omega}}_{\mathrm{d}} \otimes \hat{q}_{\mathrm{e}}\right) \times \hat{\mathbf{M}}_0 \left(\hat{\boldsymbol{\omega}}_{\mathrm{e}} + \hat{q}_{\mathrm{e}}^{*} \otimes \hat{\boldsymbol{\omega}}_{\mathrm{d}} \otimes \hat{q}_{\mathrm{e}}\right) \\ & - \hat{\mathbf{M}}_0\left(\hat{q}_{\mathrm{e}}^{*} \otimes \dot{\hat{\boldsymbol{\omega}}}_{\mathrm{d}} \otimes \hat{q}_{\mathrm{e}}\right) - \hat{\mathbf{M}}_0 \hat{\boldsymbol{\omega}}_{\mathrm{e}} \times \left(\hat{q}_{\mathrm{e}}^{*} \otimes \hat{\boldsymbol{\omega}}_{\mathrm{d}} \otimes \hat{q}_{\mathrm{e}}\right) \\ & + \hat{F}_{g0} - \hat{\beta} \odot \hat{\mathbf{M}}_0 \dot{\hat{\boldsymbol{\Omega}}}_{\mathrm{e}} - \hat{c} \odot \hat{\mathbf{M}}_0 \dot{\chi}\left(\hat{\boldsymbol{\Omega}}_{\mathrm{e}}\right). \end{aligned} \tag{25}$$

3.2. Extended-State-Observer Design. The ESO method shows very fine performance in disturbance rejection and compensation of uncertainties that the accuracy of the controller can be improved. Based on the SOSM method mentioned in References [25, 32], and by combining the linear and nonlinear correction terms, a novel extended state observer is proposed as follows:

$$\begin{cases} \hat{e}_1 = \hat{z}_1 - \hat{s}, \\ \hat{e}_2 = \hat{z}_2 - \hat{D}, \\ \dot{\hat{z}}_1 = \hat{\mathbf{M}}_0^{-1}\hat{F}_u + \hat{\mathbf{M}}_0^{-1} S\left(\hat{\boldsymbol{\omega}}_{\mathrm{e}}, \hat{q}_{\mathrm{e}}\right) - \hat{\kappa} \odot \hat{e}_1 - \hat{\eta} \odot \operatorname{sgn}^{p_2}\left(\hat{e}_1\right) + \hat{z}_2, \\ \dot{\hat{z}}_2 = -\hat{\rho} \odot \hat{e}_1 - \hat{\lambda} \odot \operatorname{sgn}^{2p_2-1}\left(\hat{e}_1\right), \end{cases} \tag{26}$$

where $\hat{z}_1 \in \mathbb{N}^3$ and $\hat{z}_2 \in \mathbb{N}^3$ are the outputs of the observer; $\hat{\mathrm{D}} = \Delta\hat{\mathrm{F}}_{\mathrm{g}} + \hat{\mathrm{F}}_{\mathrm{d}} + \Delta\hat{\Sigma}$ is the total disturbance and also the extended state variable; $\hat{e}_1$ and $\hat{e}_2$ represent the observer measurement; $p_2 \in [0.5, 1)$; $\hat{\kappa}, \hat{\eta}, \hat{\rho}, \hat{\lambda} \in \mathbb{R}^3$ are the observer designed parameters, respectively; and $S(\hat{\boldsymbol{\omega}}_{\mathrm{e}}, \hat{q}_{\mathrm{e}})$ is

$$\begin{aligned} S\left(\hat{\boldsymbol{\omega}}_{\mathrm{e}}, \hat{q}_{\mathrm{e}}\right) = \hat{\mathbf{M}}^{-1}\Big(& \hat{F}_{\mathrm{d}} + \hat{F}_g - \left(\hat{\boldsymbol{\omega}}_{\mathrm{e}} + \hat{q}_{\mathrm{e}}^{*} \otimes \hat{\boldsymbol{\omega}}_{\mathrm{d}} \otimes \hat{q}_{\mathrm{e}}\right) \\ & \times \hat{\mathbf{M}}\left(\hat{\boldsymbol{\omega}}_{\mathrm{e}} + \hat{q}_{\mathrm{e}}^{*} \otimes \hat{\boldsymbol{\omega}}_{\mathrm{d}} \otimes \hat{q}_{\mathrm{e}}\right) - \hat{\mathbf{M}}\left(\hat{q}_{\mathrm{e}}^{*} \otimes \dot{\hat{\boldsymbol{\omega}}}_{\mathrm{d}} \otimes \hat{q}_{\mathrm{e}}\right) \\ & + \hat{\mathbf{M}}\hat{\boldsymbol{\omega}}_{\mathrm{e}} \times \left(\hat{q}_{\mathrm{e}}^{*} \otimes \hat{\boldsymbol{\omega}}_{\mathrm{d}} \otimes \hat{q}_{\mathrm{e}}\right)\Big). \end{aligned} \tag{27}$$

The proposed ESO (26) can not only obtain the feature of SOSM, such as finite-time convergence but also weaken the chattering of conventional first-order sliding mode also. In addition, it inherits the best properties of linear and nonlinear correction terms. Then, the error dynamics can be established from equation (26) in the scalar form:

$$\begin{cases} \dot{\widehat{e}}_1 = \widehat{e}_2 - \widehat{\kappa} \odot \widehat{e}_1 - \widehat{\eta} \odot \operatorname{sgn}^{p_2}(\widehat{e}_1), \\ \dot{\widehat{e}}_2 = -\widehat{\rho} \odot \widehat{e}_1 - \widehat{\lambda} \odot \operatorname{sgn}^{2p_2-1}(\widehat{e}_1) - \dot{\widehat{g}}_i(t), \end{cases} \tag{28}$$

where $\dot{\widehat{g}}_i(t)$ is the derivative of $\widehat{D}$ and the amplitude of $\dot{\widehat{g}}_i(t)$ is assumed to be bounded by a positive value $\overline{g}$, that is $|\dot{\widehat{g}}_i(t)| \le \overline{g}$.

Based on the NTSMC and ESO designed above, the integral controller is designed as

$$\widehat{F}_u^{\mathrm{f}} = \widehat{F}_{\mathrm{e}} + \widehat{F}_s + \widehat{F}_\tau, \tag{29}$$

where $\widehat{F}_{\mathrm{e}}$, $\widehat{F}_s$, and $\widehat{F}_\tau$ are given by

$$\begin{aligned} \widehat{F}_{\mathrm{e}} &= (\widehat{\boldsymbol{\omega}}_{\mathrm{e}} + \widehat{q}_{\mathrm{e}}^* \otimes \widehat{\boldsymbol{\omega}}_{\mathrm{d}} \otimes \widehat{q}_{\mathrm{e}}) \times \widehat{\mathbf{M}}_0 (\widehat{\boldsymbol{\omega}}_{\mathrm{e}} + \widehat{q}_{\mathrm{e}}^* \otimes \widehat{\boldsymbol{\omega}}_{\mathrm{d}} \otimes \widehat{q}_{\mathrm{e}}) \\ &\quad + \widehat{\mathbf{M}}_0 \left(\widehat{q}_{\mathrm{e}}^* \otimes \dot{\widehat{\boldsymbol{\omega}}}_{\mathrm{d}} \otimes \widehat{q}_{\mathrm{e}}\right) - \widehat{\mathbf{M}}_0 \widehat{\boldsymbol{\omega}}_e \times (\widehat{q}_{\mathrm{e}}^* \otimes \widehat{\boldsymbol{\omega}}_{\mathrm{d}} \otimes \widehat{q}_{\mathrm{e}}) \\ &\quad + \widehat{F}_{g0} - \widehat{\beta} \odot \dot{\widehat{\boldsymbol{\Omega}}}_{\mathrm{e}} - \widehat{c} \odot \dot{\chi}\left(\widehat{\boldsymbol{\Omega}}_{\mathrm{e}}\right), \\ \widehat{F}_s &= -\widehat{k} \odot sig^{p_1}(\widehat{s}), \\ \widehat{F}_\tau &= -\widehat{z}_2. \end{aligned} \tag{30}$$

Under the proposed controller in equations (29) and (30), the control objective can be achieved for tracking tumbling target. The closed-loop system for coupled rotational and translational control is shown in Figure 3.

4. Stability Analysis

In this section, the stability analysis is divided into two parts. In the first part (Theorem 1), the finite-time convergence of ESO is proved, which implies that the proposed ESO can estimate the exact state and total disturbances within a fixed time. In the second part (Theorem 2), the finite-time stability of the closed-loop system is proved, which indicates that the finite-time convergence of the tracking error $(\widehat{\boldsymbol{\Omega}}_{\mathrm{e}}, \widehat{\boldsymbol{\omega}}_{\mathrm{e}})$ can be obtained. The proofs of finite-time convergence of ESO and total closed-loop system will be given using Lyapunov stability theory.

Theorem 1. *Suppose the parameters of ESO in equation (26) satisfy the following:*

$$p_1 \widehat{\lambda} \widehat{\rho} > \widehat{\kappa}^2 \widehat{\lambda} + p_2 (p_2 + 1)^2 \widehat{\eta}^2 \widehat{\kappa}^2. \tag{31}$$

Then, the observer errors will converge to the following region in finite-time:

$$\boldsymbol{\Omega}_1 = \left\{ \vartheta \mid \|\vartheta\| \le \delta = \left(\frac{\overline{g}\|\mathbf{R}\|}{\lambda_{\min}(\mathbf{Q}_1)} \right)^{p_2/2p_2-1} \right\}, \tag{32}$$

where $\vartheta = [\|\widehat{e}_{1i}\|^{p_2} \operatorname{sgn}(\widehat{e}_{1i}), \widehat{e}_{1i}, \widehat{e}_{2i}]^{\mathrm{T}}$, $\mathbf{R} = [\,\widehat{\eta} \;\; \widehat{\kappa} \;\; -2\,]$, and the matrix $\mathbf{Q}_1$ satisfies the following expression:

$$\mathbf{Q}_1 = \eta \begin{bmatrix} \widehat{\lambda} + p_1 \widehat{\eta}^2 & 0 & -p_1 \widehat{\eta} \\ 0 & \widehat{\rho} + (2 + p_1)\widehat{\kappa}^2 & -(p_1 + 1)\widehat{\kappa} \\ -p_1 \widehat{\eta} & -(p_1 + 1)\widehat{\kappa} & p_1 \end{bmatrix}. \tag{33}$$

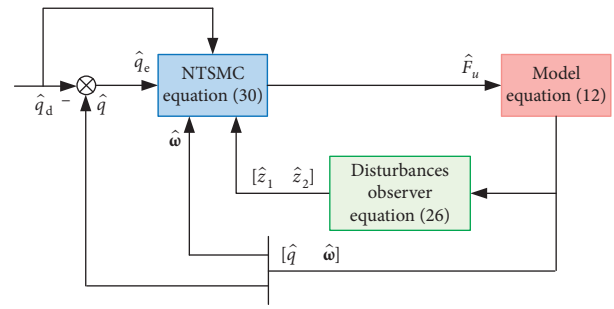

Figure 3: Closed-loop system of NTSMC-ESO for spacecraft coupled control.

The convergence time is upperbounded by $t_m \le 2/\theta_1 \ln((\theta_1 V_0^{(1/2)} + \theta_2)/\theta_2)$, where V_0 is the initial Lyapunov state and θ_1 and θ_2 are the constants depending on the gains.

Proof. To verify the finite-convergence performance, in accordance with the idea of Moreno and Osorio [25], a Lyapunov candidate is proposed as

$$\begin{aligned} V_1 &= \frac{1}{2}\left(\widehat{\eta} \odot |\widehat{e}_{1i}|^{p_2} \operatorname{sgn}(\widehat{e}_{1i}) + \widehat{\kappa} \odot \widehat{e}_{1i} - \widehat{e}_{2i}\right)^{\mathrm{T}} \\ &\quad \cdot \left(\widehat{\eta} \odot |\widehat{e}_{1i}|^{p_2} \operatorname{sgn}(\widehat{e}_{1i}) + \widehat{\kappa} \odot \widehat{e}_{1i} - \widehat{e}_{2i}\right) + \frac{\widehat{\lambda}}{p_1} \odot |\widehat{e}_{1i}|^{2p_2} \\ &\quad + \widehat{\rho} \odot \widehat{e}_{1i}^T \widehat{e}_{1i} + \frac{1}{2} \widehat{e}_{2i}^T \widehat{e}_{2i}, \\ &= \vartheta^T \Gamma \vartheta, \end{aligned} \tag{34}$$

where $\vartheta = [|\widehat{e}_{1i}|^{p_2} \operatorname{sgn}(\widehat{e}_{1i}), \widehat{e}_{1i}, \widehat{e}_{2i}]^{\mathrm{T}}$ and the matrix Γ is defined as

$$\Gamma = \frac{1}{2} \begin{bmatrix} 2\widehat{\lambda}/p_1 + \widehat{\eta}^2 & \widehat{\eta}\widehat{\kappa} & -\widehat{\eta} \\ \widehat{\eta}\widehat{\kappa} & 2\widehat{\rho} + \widehat{\kappa}^2 & -\widehat{\kappa} \\ -\widehat{\eta} & -\widehat{\kappa} & 2 \end{bmatrix}. \tag{35}$$

It is obvious that V_1 is positive definite and radially unbounded if $\widehat{\lambda}$ and $\widehat{\rho}$ are positive. The range of V_1 is obtained as follows:

$$\lambda_{\min}(\Gamma)\|\vartheta\|^2 \le V_1 \le \lambda_{\max}(\Gamma)\|\vartheta\|^2, \tag{36}$$

where $\|\vartheta\|^2 = |\widehat{e}_{1i}|^{2p_2} + \widehat{e}_{1i}^{\mathrm{T}}\widehat{e}_{1i} + \widehat{e}_{2i}^{\mathrm{T}}\widehat{e}_{2i}$ is the Euclidean norm of ϑ and $\lambda_{\min}(\cdot)$ and $\lambda_{\max}(\cdot)$ represent the minimum and maximum eigenvalues of the matrix, respectively.

The time derivative of V_1 can be obtained as

$$\begin{aligned} \dot{V}_1 &= \left(2\widehat{\lambda} + p_1\widehat{\eta}^2\right) \odot |\widehat{e}_{1i}|^{2p_2-1} \dot{\widehat{e}}_{1i} \operatorname{sgn}(\widehat{e}_{1i}) + \left(2\widehat{\rho} + \widehat{\kappa}^2\right) \odot \widehat{e}_{1i}^{\mathrm{T}} \dot{\widehat{e}}_{1i} \\ &\quad + 2\widehat{e}_{2i}^{\mathrm{T}} \dot{\widehat{e}}_{2i} + (p_1 + 1)\widehat{\eta}\widehat{\kappa} \odot |\widehat{e}_{1i}|^{p_2} \dot{\widehat{e}}_{1i} \operatorname{sgn}(\widehat{e}_{1i}) \\ &\quad - p_1 \widehat{\eta} \odot |\widehat{e}_{1i}|^{p_2-1} \dot{\widehat{e}}_{1i}^{\mathrm{T}} \widehat{e}_{2i} - \widehat{\eta} \odot |\widehat{e}_{1i}|^{p_2} \operatorname{sgn}(\widehat{e}_{1i}) \dot{\widehat{e}}_{2i} \\ &\quad - \widehat{\kappa} \odot \dot{\widehat{e}}_{1i}^{\mathrm{T}} \widehat{e}_{2i} - \widehat{\kappa} \odot \widehat{e}_{1i}^{\mathrm{T}} \dot{\widehat{e}}_{2i}. \end{aligned} \tag{37}$$

Substituting equation (28) into equation (37) yields

$$\begin{aligned}\dot{V}_1 &= \left|\hat{e}_{1i}\right|^{p_2-1}\Big[-\left(\hat{\eta}\lambda+\hat{\eta}p_2\hat{\eta}^2\right)\left|\hat{e}_{1i}\right|^{2p_2}-\left(\hat{\eta}\hat{\rho}+(2+p_2)\hat{\eta}\hat{\kappa}^2\right)\left|\hat{e}_{1i}\right|^2\\ &\quad -p_1\hat{\eta}\odot\hat{e}_{2i}^{\mathrm{T}}\hat{e}_{2i}+2(p_2+1)\hat{\eta}\hat{\kappa}\odot\hat{e}_{1i}^{\mathrm{T}}\hat{e}_{2i}\\ &\quad +2p_2\hat{\eta}^2\odot\left|\hat{e}_{1i}\right|^{p_2}\operatorname{sgn}\left(\hat{e}_{1i}\right)\hat{e}_{2i}\Big]+\Big[-\hat{\kappa}\odot\hat{e}_{2i}^{T}\hat{e}_{2i}-\left(\hat{\kappa}\hat{\rho}+\hat{\kappa}^3\right)\\ &\quad \odot\hat{e}_{2i}^{\mathrm{T}}\hat{e}_{2i}-\left(\hat{\kappa}\hat{\lambda}+2\hat{\kappa}p_2\hat{\eta}^2+\hat{\eta}^2\hat{\kappa}\right)\left|\hat{e}_{1i}\right|^{2p_2}+2\hat{\kappa}^2\odot\hat{e}_{1i}^{\mathrm{T}}\hat{e}_{2i}\\ &\quad +\left[\hat{\eta}\odot\left|\hat{e}_{1i}\right|^{p_2}\operatorname{sgn}\left(\hat{e}_{1i}\right)-2\hat{e}_{2i}+\hat{\kappa}\hat{e}_{1i}\right]\hat{g}_i(t),\\ &= -\left|\hat{e}_{1i}\right|^{p_2-1}\vartheta^{\mathrm{T}}\mathbf{Q}_1\vartheta-\vartheta^{\mathrm{T}}\mathbf{Q}_2\vartheta+\hat{g}_i(t)\mathbf{R}\vartheta,\end{aligned}\tag{38}$$

where the matrices $\mathbf{Q}_1$, $\mathbf{Q}_2$, and $\mathbf{R}$ are given by

$$\begin{aligned}\mathbf{Q}_1 &= \hat{\eta}\begin{bmatrix}\hat{\lambda}+p_2\hat{\eta}^2 & 0 & -p_2\hat{\eta}\\ 0 & \hat{\rho}+(2+p_2)\hat{\kappa}^2 & -(p_2+1)\hat{\kappa}\\ -p_2\hat{\eta} & -(p_2+1)\hat{\kappa} & p_2\end{bmatrix},\\ \mathbf{Q}_2 &= \hat{\kappa}\begin{bmatrix}\hat{\lambda}+(2p_2+1)\hat{\eta}^2 & 0 & 0\\ 0 & \hat{\rho}+\hat{\kappa}^2 & -\hat{\kappa}\\ 0 & -\hat{\kappa} & 1\end{bmatrix},\\ \mathbf{R} &= \begin{bmatrix}\hat{\eta} & \hat{\kappa} & -2\end{bmatrix}.\end{aligned}\tag{39}$$

It is obvious that $\mathbf{Q}_2$ is a symmetric matrix, and if λ and κ are positive, it is positive definite. In addition, calculate the determinant of $\mathbf{Q}_1$ as

$$\begin{aligned}\left\|\mathbf{Q}_1\right\| &= p_2\left(\hat{\lambda}+p_2\hat{\eta}^2\right)\left\{\left[\hat{\rho}+(2+p_2)\hat{\kappa}^2-(p_2+1)^2\hat{\kappa}^2\right]\right\}\\ &\quad -p_2^2\hat{\eta}^2\left[\hat{\rho}+(2+p_2)\hat{\kappa}^2\right],\\ &= \hat{\lambda}\left[p_2\hat{\rho}+p_2(2+p_2)\hat{\kappa}^2-(p_2+1)^2\hat{\kappa}^2\right]\\ &\quad -p_2\hat{\eta}^2(p_2+1)^2\hat{\kappa}^2,\\ &= \hat{\lambda}\left(p_2\hat{\rho}-\hat{\kappa}^2\right)-p_2\hat{\eta}^2(p_2+1)^2\hat{\kappa}^2.\end{aligned}\tag{40}$$

Substituting equation (31) into equation (40), it yields $\|\mathbf{Q}_1\|>0$. Therefore, $\mathbf{Q}_1$ is the positive definite matrix. According to the definition of ϑ, it can be obtained that

$$\left|\hat{e}_{1i}\right|^{p_2-1}\geq\|\vartheta\|^{(p_2-1/p_2)}.\tag{41}$$

According to equations (34)–(41), one obtains

$$\begin{aligned}\dot{V}_1 &= -\left|e_{1i}\right|^{p_2-1}\lambda_{\min}(\mathbf{Q}_1)\|\vartheta\|^2-\lambda_{\min}(\mathbf{Q}_2)\|\vartheta\|^2+\overline{g}\|\mathbf{R}\|\|\vartheta\|\\ &\leq -\lambda_{\min}(\mathbf{Q}_1)\|\vartheta\|^{(p_2-1/p_2)}\|\vartheta\|-\lambda_{\min}(\mathbf{Q}_2)\|\vartheta\|^2+\overline{g}\|\mathbf{R}\|\|\vartheta\|\\ &\leq -\left(c_1\|\vartheta\|^{(2p_2-1/p_2)}-c_3\right)V_1^{(1/2)}-c_2V_1,\end{aligned}\tag{42}$$

where $c_1=\lambda_{\min}(\mathbf{Q}_1)/\sqrt{\lambda_{\max}(\Gamma)}$, $c_2=\lambda_{\min}(\mathbf{Q}_2)/\lambda_{\max}(\Gamma)$, and $c_3=\overline{g}\|\mathbf{R}\|/\sqrt{\lambda_{\min}(\Gamma)}$. Based on equation (36), we assume that $V_1\geq(c_3/c_1)^{(2p_2/2p_2-1)}\lambda_{\max}(\Gamma)$, which implies that $c_1\|\vartheta\|^{(2p_2-1/p_2)}-c_3\geq 0$. And it is obvious that $c_2>0$. By substituting $\theta_1=c_1\|\vartheta\|^{(2p_2-1/p_2)}-c_3$ and $\theta_2=c_2$ into equation (42), one obtains

$$\dot{V}_1\leq -\theta_1V_1^{(1/2)}-\theta_2V_1.\tag{43}$$

Therefore, according to Lemma 2, it is obvious that $\dot{V}_1$ is definitely negative and V_1 is positive. Therefore, observer error will converge to the small set $\mathbf{\Omega}_1$ in finite time and the convergence time satisfies $t_m\leq 2/\theta_1\ln(\theta_1V_0^{(1/2)}+\theta_2)/(\theta_2)$. The proof of Theorem 1 is completed. □

Remark 3. As seen in Theorem 1 and its proof, the reconstruction error of the model uncertainties and external disturbances can be driven to the neighborhoods of the origin in finite time. The parameter $(p_2/2p_2-1)$ gets larger, and the region $\mathbf{\Omega}_1=\left\{\vartheta\,|\,\|\vartheta\|\leq\delta=(\overline{g}\|\mathbf{R}\|/\lambda_{\min}(\mathbf{Q}_1))^{(p_2/2p_2-1)}\right\}$ will be smaller by choosing adequate ESO parameters, p_2, $\hat{\kappa}$, $\hat{\eta}$, $\hat{\rho}$, and $\hat{\lambda}$, which implies that the proposed ESO has high accuracy. In this way, the output of observer will not influence the controller. Therefore, the finite-time convergence of the closed-loop system, mentioned in Theorem 2, is proved on the basis of Theorem 1. Some studies containing ESO-NTSMC analyzed the total finite-time convergence of the closed-loop system in the same way [32, 33].

Theorem 2. *Based on the estimated state in observer (26), and with the application of the controller in equations (29) and (30), the close-loop system states will be driven to a neighborhood of the sliding surface $\hat{s}=\hat{0}$ in finite time. Moreover, the tracking errors $\hat{\mathbf{\Omega}}_e$ and $\hat{\boldsymbol{\omega}}_e$ will converge to a small region in finite time.*

Proof. The proof includes two consecutive steps:

Firstly, it is to be proved that the sliding surface will converge to $\hat{s}=\hat{0}$ in finite time. Define the form of the Lyapunov function as follows:

$$V_2=\frac{1}{2}\hat{s}^{\mathrm{T}}\hat{\mathbf{M}}\hat{s}.\tag{44}$$

Taking the time derivative of $\hat{s}$ in equation (20), it yields

$$\dot{\hat{s}}=-\hat{\mathbf{M}}^{-1}\left(\hat{F}_u+\hat{D}\right)-\hat{\mathbf{M}}^{-1}S\left(\hat{\boldsymbol{\omega}}_{\mathrm{e}},\hat{q}_{\mathrm{e}}\right)+\hat{\beta}\odot\dot{\hat{\mathbf{\Omega}}}_{\mathrm{e}}+\hat{c}\odot\dot{\chi}\left(\hat{\mathbf{\Omega}}_{\mathrm{e}}\right).\tag{45}$$

With the application of equations (29) and (30), $\dot{\hat{s}}$ can be obtained as

$$\dot{\hat{s}}=\hat{\mathbf{M}}^{-1}\left(-\hat{k}\odot\operatorname{sig}^{p_1}(\hat{s})-\hat{z}_2+\hat{D}\right).\tag{46}$$

Take the time derivative of V_2 yields

$$\begin{aligned}\dot{V}_2 &= \hat{s}^{\mathrm{T}}\hat{\mathbf{M}}\dot{\hat{s}},\\ &= \hat{s}^{\mathrm{T}}\left[-\hat{k}\odot\operatorname{sig}^{p_1}(\hat{s})-\hat{z}_2+\hat{D}\right],\\ &= \hat{s}^{\mathrm{T}}\left[-\hat{k}\odot\operatorname{sig}^{p_1}(\hat{s})-\hat{e}_2\right],\end{aligned}\tag{47}$$

where $\hat{D}=\Delta\hat{F}_{\mathrm{g}}+\hat{F}_{\mathrm{d}}+\Delta\hat{\Sigma}$ is the total external disturbance and model uncertainty and $\hat{e}_2=\hat{z}_2-\hat{D}$ is the error state of ESO. Recalling from the stability in Theorem 1, the ESO errors can enter the small set $\mathbf{\Omega}$ in fixed time t_m. After finite-time t_m, the ESO errors satisfy $\|\hat{e}_2\|<\delta$. In consequence, it can be obtained as

$$\begin{aligned}\dot{V}_2 &= -\hat{s}^{\mathrm{T}}\left[\hat{k}\odot \mathrm{sig}^{p_1}(\hat{s})+\hat{e}_2\right] \le -\hat{s}^{\mathrm{T}}\left[\hat{k}\odot \mathrm{sig}^{p_1}(\hat{s})-\delta\right]\\ &\le -\sum_{i=1}^{3}\left[\left(k_i-\delta|s_i|^{-p_1}\right)|s_i|^{p_1+1}+\left(k_i'-\delta|s_i'|^{-p_1}\right)|s_i'|^{p_1+1}\right]\\ &\le -\theta_3\left(\|s\|^{p_1+1}+\|s'\|^{p_1+1}\right),\end{aligned} \tag{48}$$

where $\theta_3 = \min[(k_i-\delta|s_i|^{-p_1}), (k_i'-\delta|s_i'|^{-p_1})]$, $i = 1, 2, 3,$ is the positive scalar. For equation (48), if $\theta_3 > 0$, that is, $k_i - \delta|s_i|^{-p_1} > 0$ or $k_i' - \delta|s_i'|^{-p_1} > 0$, then one can obtain

$$\dot{V}_2 \le -\theta_4 V_2^{\left(p_1+(1/2)\right)}, \tag{49}$$

where $\theta_4 = \theta_3\sqrt{2/\max\{\sigma_{\max}(J_{\mathrm{f}}), m_{\mathrm{f}}\}}$ is a positive number. Therefore, it can be proved by Lemma 1 that the sliding surface $\hat{s}$ will converge to the set $\boldsymbol{\Omega}_2 = \{\hat{s}|\|\hat{s}\| \le \Delta_s = (\|\hat{k}\|/\delta)^{p_1}\}$ in finite time.

Secondly, when the close-loop system state reaches the neighborhood of $\hat{s} = \hat{0}$, it should be proved that the tracking error $\hat{\boldsymbol{\Omega}}_{\mathrm{e}}$ and $\hat{\boldsymbol{\omega}}_{\mathrm{e}}$ will converge into small regions containing the origin $(\hat{0}, \hat{0})$ in finite time. Due to different conditions of $\hat{s}$ and $\hat{\boldsymbol{\Omega}}_{\mathrm{e}}$ in (23), the following cases should be taken into consideration. □

Case 1. If $\bar{\bar{s}} = 0$, equation (20) becomes

$$\hat{\boldsymbol{\omega}}_{ei} = -\hat{\beta}_i\odot\hat{\boldsymbol{\Omega}}_{ei} - \hat{c}_i\odot\chi\left(\hat{\boldsymbol{\Omega}}_{ei}\right), \quad i = 1, 2, 3. \tag{50}$$

Consider the following Lyapunov function

$$V_3 = \langle\hat{\boldsymbol{\Omega}}_{\mathrm{e}}, \hat{\boldsymbol{\Omega}}_{\mathrm{e}}\rangle. \tag{51}$$

Taking the time derivative of V_3 yields

$$\begin{aligned}\dot{V}_3 &= \langle\hat{\boldsymbol{\Omega}}_{\mathrm{e}}, \dot{\hat{\boldsymbol{\Omega}}}_{\mathrm{e}}\rangle = \langle\hat{\boldsymbol{\Omega}}_{\mathrm{e}}, \hat{\boldsymbol{\omega}}_{\mathrm{e}}\rangle,\\ &= \left\langle\hat{\boldsymbol{\Omega}}_{\mathrm{e}}, -\hat{\beta}_i\odot\hat{\boldsymbol{\Omega}}_{\mathrm{e}} - \hat{c}\odot\left[\mathrm{sgn}(\boldsymbol{\Omega}_{\mathrm{e}})|\boldsymbol{\Omega}_{\mathrm{e}}|^{\alpha} + \varepsilon\mathrm{sgn}(\mathbf{p}_{\mathrm{e}})|\mathbf{p}_{\mathrm{e}}|^{\alpha}\right]\right\rangle,\\ &= -\hat{\beta}\langle\hat{\boldsymbol{\Omega}}_{\mathrm{e}}, \hat{\boldsymbol{\Omega}}_{\mathrm{e}}\rangle - \sum_{i=1}^{3}\left(c_i|\boldsymbol{\Omega}_{ei}|^{\alpha+1} + c_i'|\mathbf{p}_{ei}|^{\alpha+1}\right)\\ &\le -\theta_5 V_3 - \theta_6 V_3^{(1+\alpha/2)},\end{aligned} \tag{52}$$

Table 1: Simulation experiment parameters.

Orbital elements	Values
Semimajor axis (km)	6778
Eccentricity	0.02
Inclination (deg)	45
Right ascension of the ascending node (deg)	30
Argument of perigee (deg)	25
True anomaly (deg)	30

Table 2: Control gains for simulations.

Controllers	Controller gains
ESO-NTSMC	$\alpha = 0.67$; $\mu = 10^{-3}$; $\hat{\beta} = 0.15 + \varepsilon 2$; $\hat{c} = 0.2 + \varepsilon 0.5$; $\hat{k} = 20 + \varepsilon 10$; $\hat{\eta} = 3 + \varepsilon 1$; $\hat{\kappa} = 10 + \varepsilon 5$; $\hat{\lambda} = 3 + \varepsilon 0.9$; $\hat{\rho} = 0.01 + \varepsilon 0.01$; $p_1 = 0.6$; $p_2 = 0.6$
LESO-NTSMC	$\alpha = 0.67$; $\mu = 10^{-3}$; $\hat{\beta} = 0.15 + \varepsilon 2$; $\hat{c} = 0.2 + \varepsilon 0.5$; $\hat{k} = 20 + \varepsilon 10$;$\hat{\kappa} = 10 + \varepsilon 5$; $\hat{\rho} = 0.01 + \varepsilon 0.01$; $p_1 = 0.6$; $p_2 = 0.6$
ESO-TSM	$\alpha = 5/3$; $\hat{\beta} = 0.5 + \varepsilon 0.8$; $\hat{k} = 20 + \varepsilon 10$; $\hat{\eta} = 3 + \varepsilon 1$; $\hat{\kappa} = 10 + \varepsilon 5$; $\hat{\lambda} = 3 + \varepsilon 0.9$; $\hat{\rho} = 0.01 + \varepsilon 0.01$; $p_1 = 0.6$; $p_2 = 0.6$

where $\theta_5 = \hat{\beta}$ and $\theta_6 = \min(c_i, c_i')$, $i = 1, 2, 3$ are the parameters.

Therefore, according to Lemma 2, the error states $\hat{\boldsymbol{\Omega}}_{\mathrm{e}}$ and $\hat{\boldsymbol{\omega}}_{\mathrm{e}}$ will converge to $(\hat{0}, \hat{0})$ in finite time.

Case 2. If $\bar{\bar{s}} \ne 0$, $|\hat{\boldsymbol{\Omega}}_{ei}| \le \varepsilon_0$, which indicates that $\hat{\boldsymbol{\Omega}}_{ei}$ converged into the set $|\hat{\boldsymbol{\Omega}}_{ei}| \le \varepsilon_0$. One can obtain

$$\hat{\boldsymbol{\omega}}_{ei} + \hat{\beta}_i\odot\hat{\boldsymbol{\Omega}}_{ei} + \hat{c}_i\odot\left(\hat{\gamma}_{1i}\odot\hat{\boldsymbol{\Omega}}_{ei} + \hat{\gamma}_{2i}\odot\mathrm{sgn}\left(\hat{\boldsymbol{\Omega}}_{ei}\right)\left|\hat{\boldsymbol{\Omega}}_{ei}\right|^2\right) = \delta_s, \quad |\delta_s| < \Delta_s. \tag{53}$$

Therefore, $\hat{\boldsymbol{\omega}}_{ei}$ will eventually converge to the region as follows:

$$\hat{\boldsymbol{\omega}}_{ei} \le |\delta_s| + \hat{\beta}_i\varepsilon_0 + \hat{c}_i\odot\left(\hat{\gamma}_{1i}\varepsilon_0 + \hat{\gamma}_{2i}\varepsilon_0^2\right). \tag{54}$$

Case 3. If $\bar{\bar{s}} \ne 0$, $|\hat{\boldsymbol{\Omega}}_{ei}| \ge \varepsilon_0$, it implies that

$$\begin{aligned}&\hat{\boldsymbol{\omega}}_{ei} + \hat{\beta}_i\odot\hat{\boldsymbol{\Omega}}_{ei} + \hat{c}_i\odot\mathrm{sig}^{\alpha}\left(\hat{\boldsymbol{\Omega}}_{ei}\right) = \delta_s, \quad |\delta_s| < \Delta_s,\\ &\hat{\boldsymbol{\omega}}_{ei} + \left(\hat{\beta}_i - \frac{\delta_s}{2\hat{\boldsymbol{\Omega}}_{ei}}\right)\odot\hat{\boldsymbol{\Omega}}_{ei} + \left(\hat{c}_i - \frac{\delta_s}{2\,\mathrm{sig}^{\alpha}\left(\hat{\boldsymbol{\Omega}}_{ei}\right)}\right)\odot\mathrm{sig}^{\alpha}\left(\hat{\boldsymbol{\Omega}}_{ei}\right) = 0, \quad |\delta_s| < \Delta_s.\end{aligned} \tag{55}$$

Once $\hat{\beta}_i > \delta_s/2\hat{\boldsymbol{\Omega}}_{ei}$ and $\hat{c}_i > \delta_s/2\,\mathrm{sig}^{\alpha}(\hat{\boldsymbol{\Omega}}_{ei})$, then $\hat{s}$ is still kept in the form of terminal sliding mode, which implies that $|\hat{\boldsymbol{\Omega}}_{ei}|$ will be bounded as $|\hat{\boldsymbol{\Omega}}_{ei}| \le \varepsilon_1 = \min\{(\Delta_s/2\beta_i), (\Delta_s/2c_i)^{(1/\alpha)}\}$.

In conclusion, $|\hat{\boldsymbol{\omega}}_{ei}|$ and $|\hat{\boldsymbol{\Omega}}_{ei}|$ will be bounded as $|\hat{\boldsymbol{\omega}}_{ei}| \le \varsigma_1$ and $|\hat{\boldsymbol{\Omega}}_{ei}| \le \varsigma_2$ in finite time, where $\varsigma_1 = |\delta_s| + \hat{\beta}_i\varepsilon_0 + \hat{c}_i\odot(\hat{\gamma}_{1i}\varepsilon_0 + \hat{\gamma}_{2i}\varepsilon_0^2)$ and $\varsigma_2 = \max\{\varepsilon_0, \varepsilon_1\}$. Based on the analysis above, it can be concluded that the control objective can be accomplished in finite time. The proof of Theorem 2 is completed.

Remark 4. The total finite-time stability of closed-loop is achieved on the basis of the above proof. With the

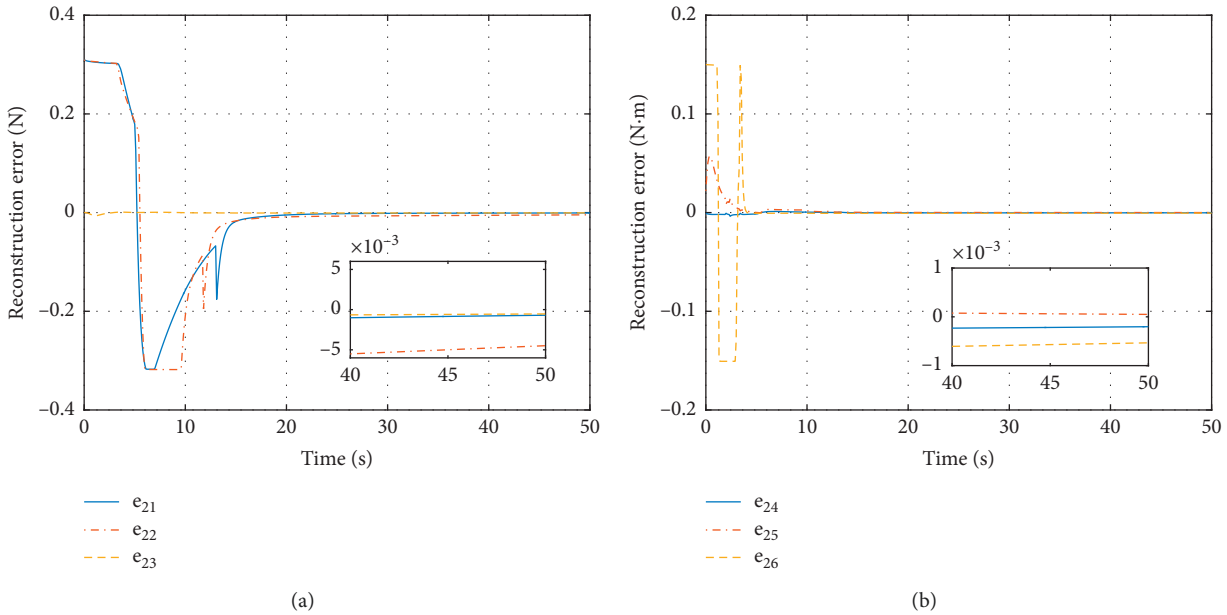

Figure 4: Time responses of reconstruction error. (a) Translational term. (b) Rotational term.

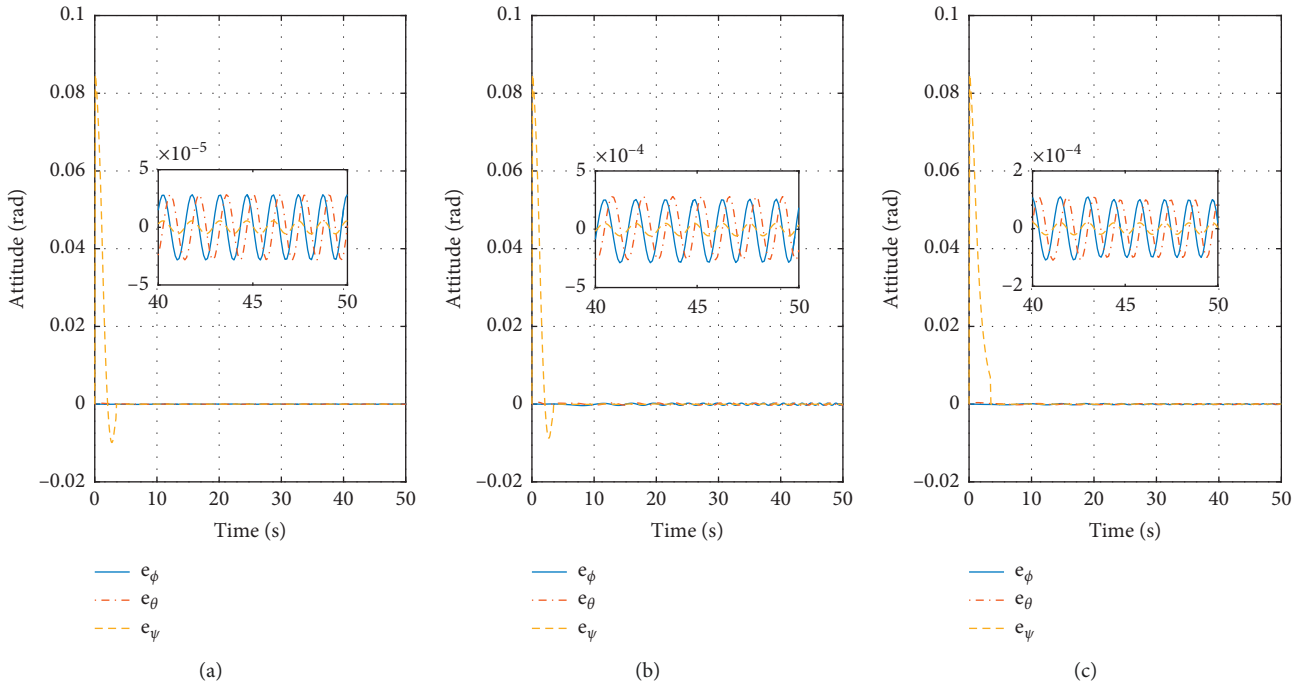

Figure 5: Time responses of relative rotation. (a) ESO NTSMC. (b) LESO NTSMC. (c) ESO TSM.

application of ESO and its estimation of total disturbances, the controller is reconstructed by adding the disturbance rejection term $\widehat{F}_\tau$ in equation (30). Therefore, the robust controller can guarantee the finite-time stability of the overall closed-loop system with high accuracy. By choosing suitable controller parameters $\widehat{k}$ and p_1 such that $\Delta_s = (\|\widehat{k}\|/\delta)^{p_1}$ is smaller enough, the convergence set $\mathbf{\Omega}_2$ can be a sufficiently small set. Therefore, it can be seen that, under the proposed controller method, the closed-loop system can achieve finite-time convergence with satisfactory performance.

Remark 5. Compared with the existing NTSMC methods, the structure of proposed controller scheme in this research combines ESO and NTSMC techniques, which can obtain higher tracking accuracy and achieve finite-time convergence. The overall controller is developed based on the estimated information of external disturbances and model

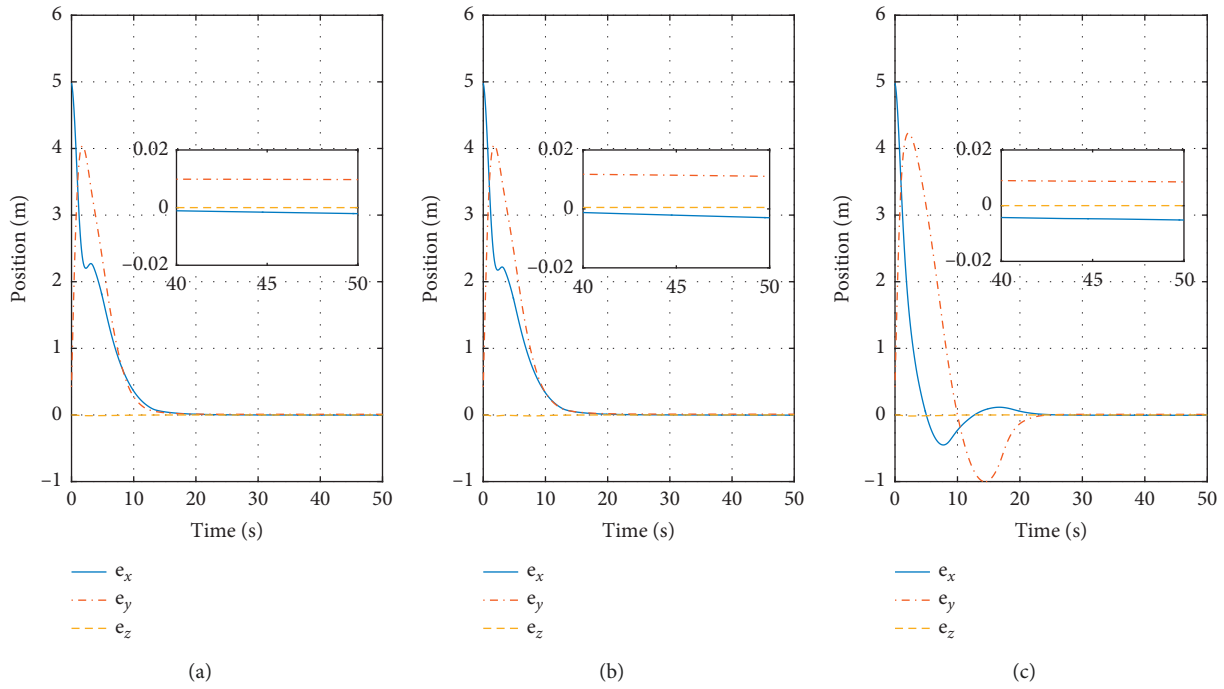

Figure 6: Time responses of relative translation. (a) ESO-NTSMC. (b) LESO-NTSMC. (c) ESO-TSM.

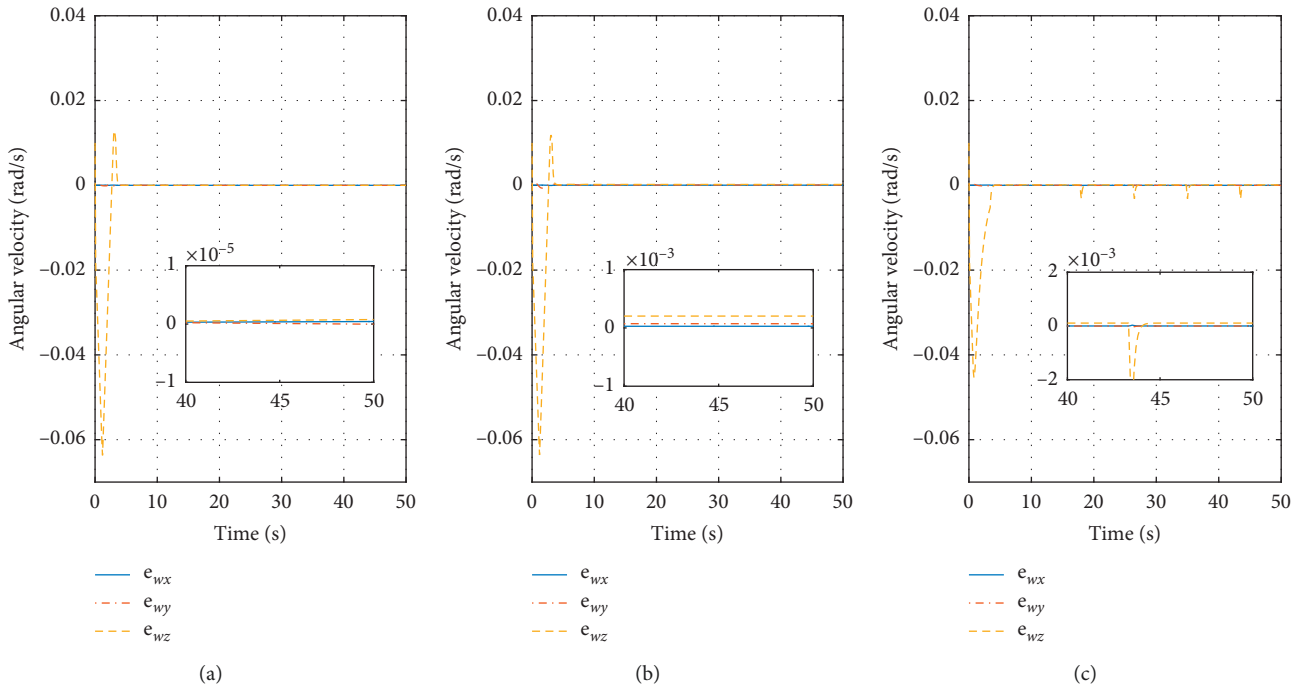

Figure 7: Time responses of relative angular velocity. (a) ESO-NTSMC. (b) LESO-NTSMC. (c) ESO-TSM.

uncertainties by ESO. Therefore, the controller does not need the priori information of perturbations. Moreover, based on the proof in equation (48), the ESO-based controller can achieve smaller steady-state error when the estimation $\hat{z}_2$ of ESO is applied to develop the robust controller, which indicates that the system has better performance and higher accuracy.

5. Simulation Results

In this section, numerical simulations are given to illustrate the effectiveness of the proposed ESO-NTSMC for the chaser tracking the tumbling target. It is assumed that the orbital elements of tumbling target are presented in Table 1. The target body-fixed frame completely coincides with the

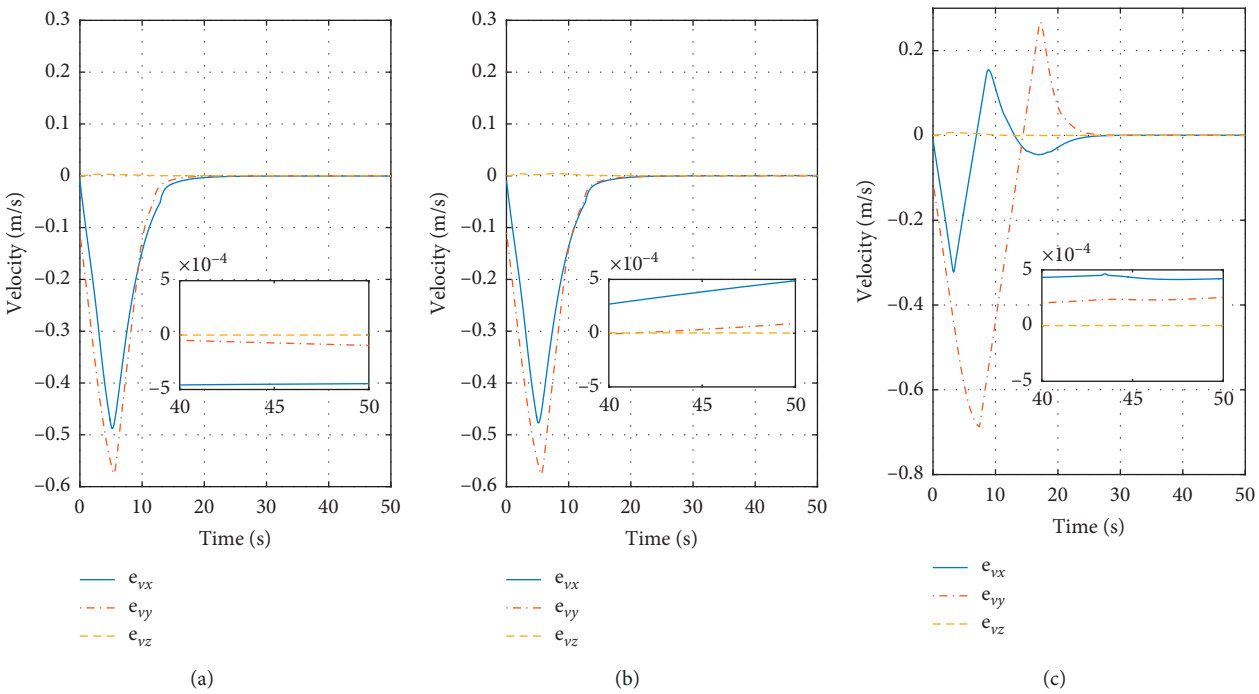

Figure 8: Time responses of relative linear velocity. (a) ESO-NTSMC. (b) LESO-NTSMC. (c) ESO-TSM.

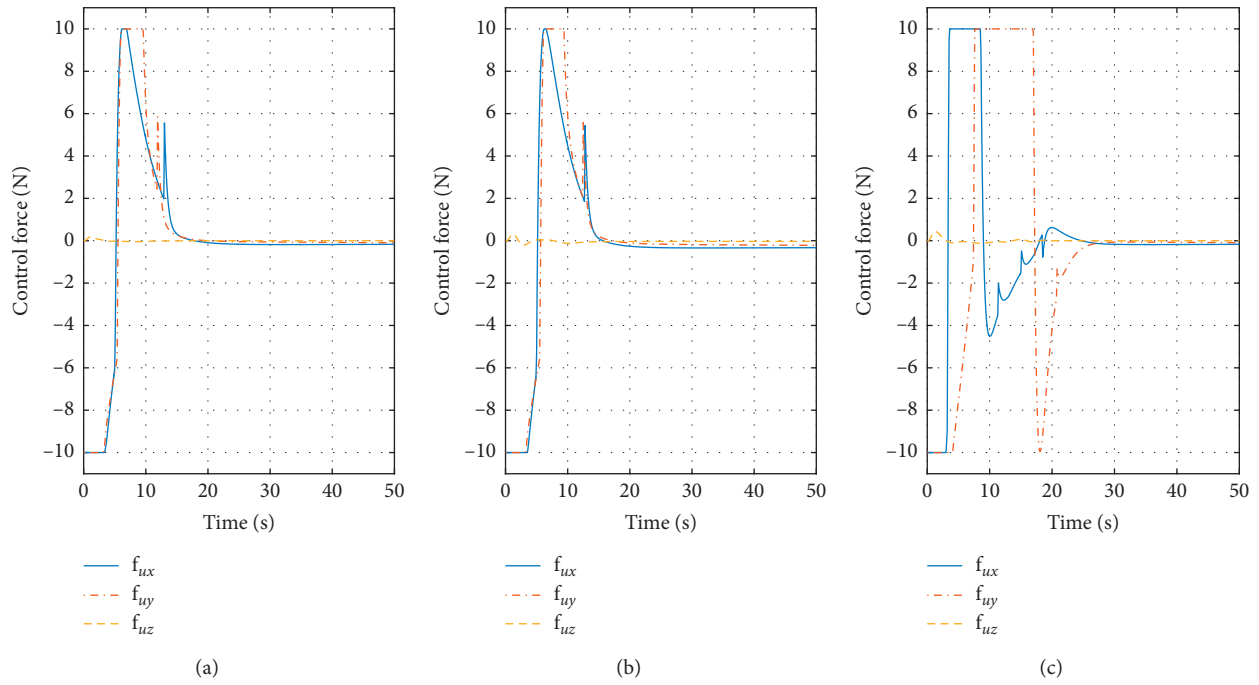

Figure 9: Time responses of control torque. (a) ESO-NTSMC. (b) LESO-NTSMC. (c) ESO-TSM.

orbital coordinate system. The control objective is to keep attitude of chaser consistent with the target, and the relative position of two can be kept at a certain distance.

The rotational angular velocity of the tumbling target is considered to be slow speed as $\boldsymbol{\omega}_t(0) = [0, 0, 0.01]^T$ (rad/s), and the capturing point in $O_l - x_l y_l z_l$ is set as $\mathbf{p}_{fl,d} = [10, 0, 0]^T$ m. The inertia matrix is supposed to be measured as $J_t = [20, 0, 0; 0, 23, 0; 0, 0, 25]$ (kg · m^2). The initial conditions of the relation motion between two spacecraft are given as $\mathbf{p}_{fl}^f(0) = [15, 0, 0]^T$ m; $q_{fl}(0) = [0.9991, 0, 0, 0.0431]^T$; and $\widehat{\boldsymbol{\omega}}_{fl}^f(0) = \widehat{0}$.

In addition, proposed NTSMC with linear-ESO, LESO-NTSMC, designed in Reference [25], and proposed ESO with conventional NTSMC, ESO-TSM, designed in Reference [38]

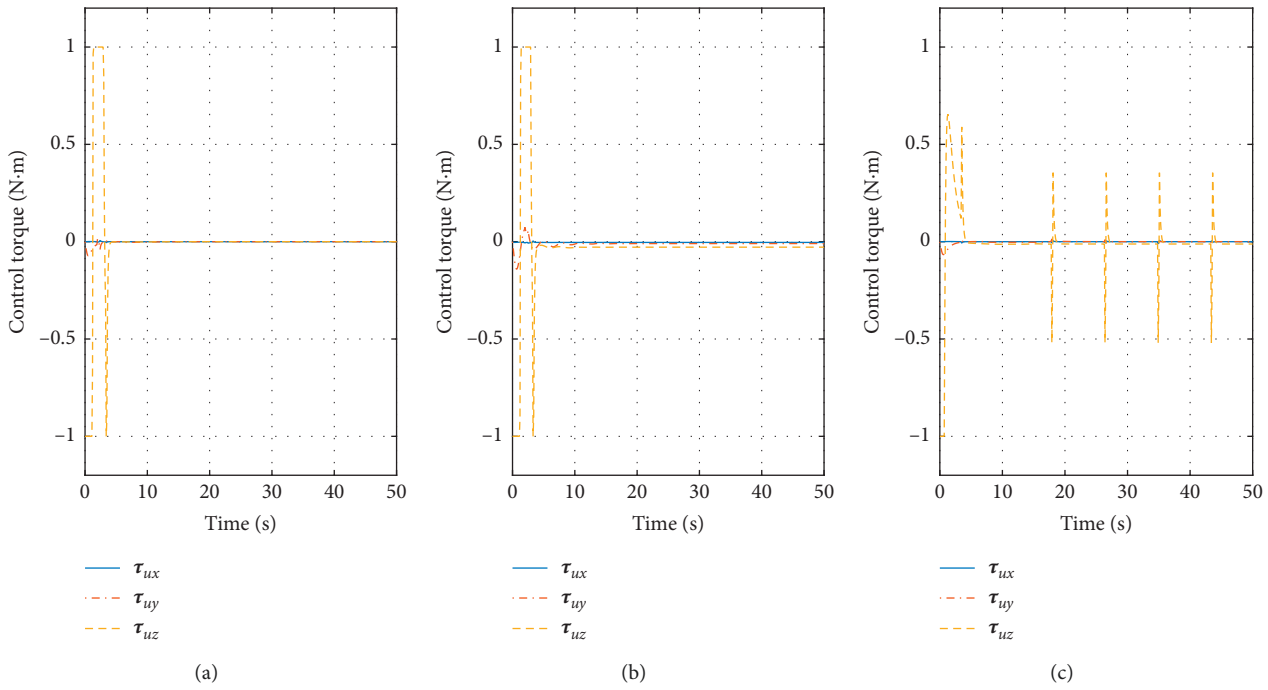

Figure 10: Time responses of control force. (a) ESO-NTSMC. (b) LESO-NTSMC. (c) ESO-TSM.

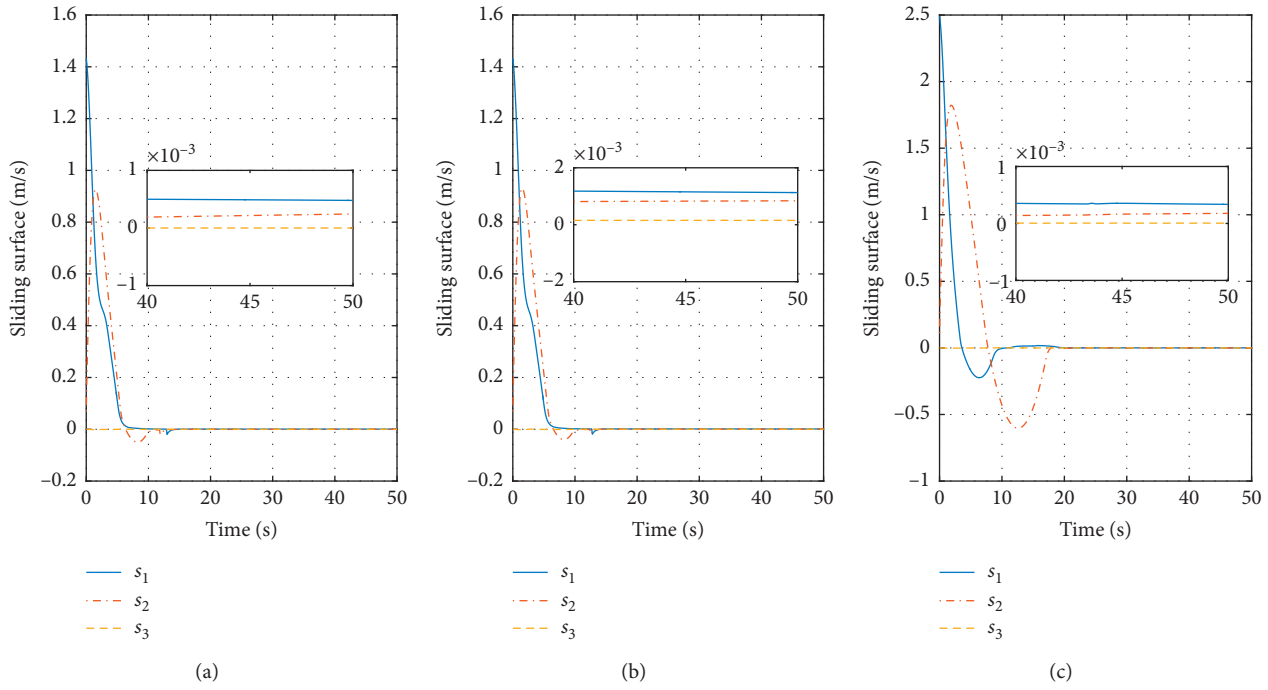

Figure 11: Time responses of sliding surface of translational term. (a) ESO-NTSMC. (b) LESO-NTSMC. (c) ESO-TSM.

are also implemented for purpose of comparison. The gains of proposed and above controllers are given in Table 2.

The preset uncertainties and disturbances are set in accordance with Reference [12]. The real mass and inertia matrix of the chaser are assumed to be $m_f = 97\,\text{kg}$ and $J_f = [18, 0, 0; 0, 17, 0; 0, 0, 20]\ (\text{kg} \cdot \text{m}^2)$. And the nominal mass and inertia matrix of the chaser is assumed to be $m_{f0} = 100\,\text{kg}$ and $J_{f0} = [22, 0, 0; 0, 20, 0; 0, 0, 23]\ (\text{kg} \cdot \text{m}^2)$, with the model uncertainties bounded by $|\Delta m_f| \le 3\,\text{kg}$ and $|J_{f,ii}| \le 3\ (\text{kg} \cdot \text{m}^2)$, $i = 1, 2, 3$, respectively. Moreover, it is assumed that the disturbance forces and torques are set as

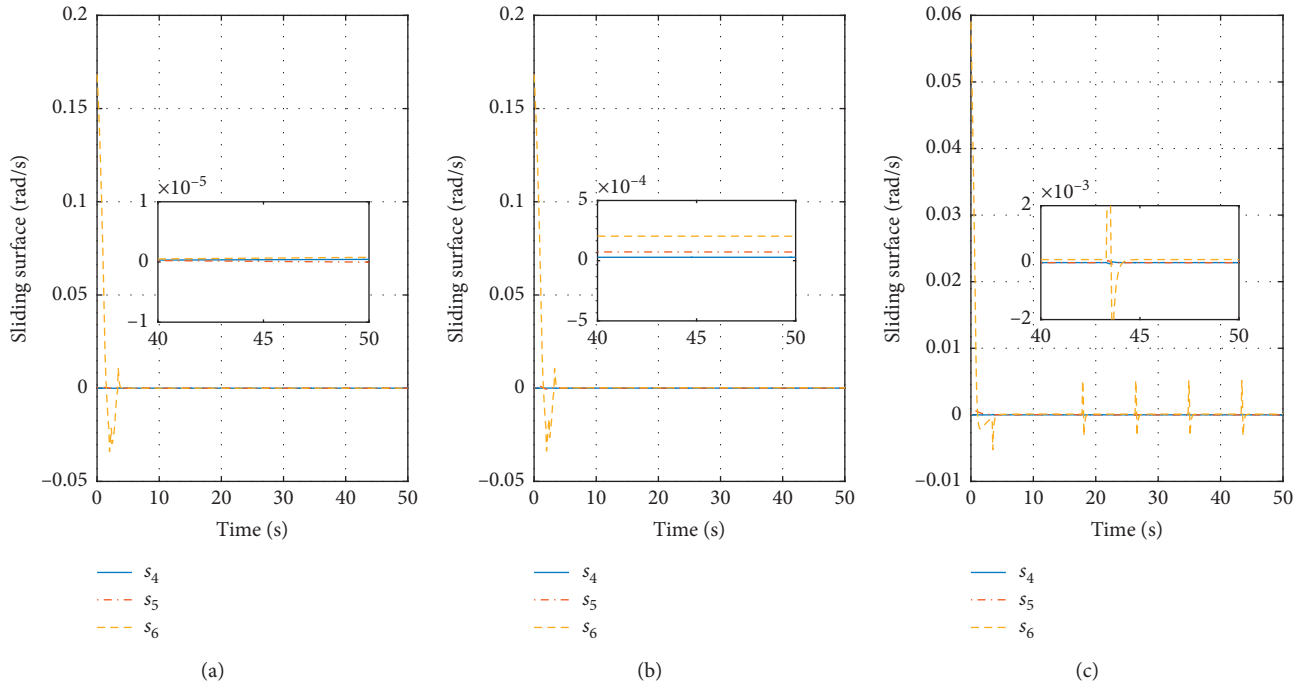

Figure 12: Time responses of sliding surface of rotational term. (a) ESO-NTSMC. (b) LESO-NTSMC. (c) ESO-TSM.

$$f_{\mathrm{d}}^{\mathrm{f}} = [0.05\cos(nt)0.07\cos(nt) - 0.01\cos(nt)]^{\mathrm{T}},$$
$$\tau_{\mathrm{d}}^{\mathrm{f}} = [-0.04\cos(nt)0.03\cos(nt) - 0.05\cos(nt)]^{\mathrm{T}}, \quad (56)$$

where $n = \pi/T_0$ is a target orbit period constant with $T_0 \approx 5711$ s. The control force is limited to the range of $|f_u| \le 10$ N, and the control torque is limited to the range of $|\tau_u| \le 1$ N·m.

Figures 4–13 show the time responses of the simulation results using the proposed ESO-NTSMC and compared control schemes, LESO-NTSMC and ESO-TSM, respectively. The results shown in Figure 4 illustrate the effectiveness of the ESO where the observer reconstruction errors of translational term and rotational term converge to a small range in finite time. In such a situation, the accuracy of the system can be enhanced when the model uncertainties and bounded external disturbances are estimated by ESO and the system can be compensated. Figures 5(a) and 6(a) shows the time responses of the tracking error of relative translation and rotation, respectively. It can be seen that the rotation error falls to tolerance within 10 s and converges to the range of 5×10^{-5} rad while the translation tracking error converges to the range of 0.02 m in around 20 s, which illustrates the performance of accuracy and rapidity of ESO-NTSMC. The time histories of relative velocity and angular velocity tracking errors are given in Figures 7(a) and 8(a), respectively. The steady-state behavior shows that the angular velocity error converges to 1×10^{-5} (rad/s) in 10 s, and the velocity error converges to 5×10^{-4} (m/s) at 20 s, which confirms the control objective of tracking the velocity of target accurately. It can be seen that, under the bounded sliding mode control force and torque shown in Figures 9(a) and 10(a), the sliding surfaces converge to the range of

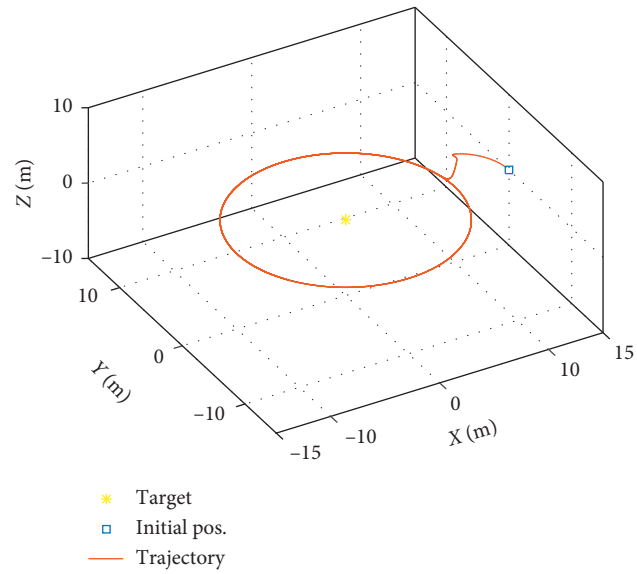

Figure 13: Trajectory of chaser tracking capturing point of tumbling target.

$|s_i| \le 1 \times 10^{-3}$ (m/s) and $|s_i'| \le 1 \times 10^{-5}$ (rad/s) in finite time successfully, which are shown in Figures 11(a) and 12(a).

The simulations of LESO-NTSMC are also carried out, which are shown in Figures 5(b)–12(b). From these figures, it can be seen that LESO-NTSMC is also tolerant to model uncertainties and external disturbances when the system states can be driven to a neighborhood of origin. As shown in Figures 11(b) and 12(b), the sliding surface accuracy of LESO-NTSMC is much lower than of ESO-NTSMC, which can illustrate that the proposed method obtains better

control ability and high control accuracy in comparison with LESO-NTSMC scheme. Figures 5(c)–12(c) show the simulation results using the ESO-based conventional NTSMC method. Severe chattering and large overshoot exist in ESO-TSM during the control process, and the convergence time of ESO-TSM is larger than the proposed one. As seen, the proposed ESO-NTSMC has faster convergence rate than ESO-TSM and can also avoid singularity. From the tracking trajectory shown in Figure 13, the chaser can successfully track the desired trajectory of docking port of tumbling target. In conclusion, it is obvious that the control object is achieved under the control strategy of proposed ESO-NTSMC while the performance and robustness can be guaranteed.

6. Conclusion

In this study, a finite-time stabilization problem of a chaser spacecraft approaching a tumbling target in presence of unknown uncertainty and bounded external disturbance has been handled. Based on the 6-DOF coupled relative motion described by dual quaternion, a combination of NTSMC and ESO is proposed to drive the translational and rotational motion to the desired state. Meanwhile, the finite-time convergence and stability property of the proposed method is rigorously proven. It was shown that the tracking error can be driven to the equilibrium point with fast response and high accuracy. Numerical simulation results show the effectiveness and performance of the proposed controller and its robustness to the model uncertainty and external disturbance.

Appendix

For a given quaternion $q = [\eta, \xi]$, η and ξ are the scalar part and the vector part, respectively. The conjugate of q is defined as $q^* = [\eta, -\xi]$ and its norm is calculated by $\|q\| = \sqrt{q \circ q^*}$. It is called unit quaternion if $\|q\| = 1$. Its logarithm is defined as

$$\ln q = \left[0, \frac{\arccos \eta}{2\sqrt{1-\eta^2}}\xi\right]. \tag{A.1}$$

The equivalent of the unit quaternion referred to Euler angle ϕ and the unit vector n is defined as

$$\ln q = \left[0, \frac{\phi}{2}n\right], \quad 0 \le \phi \le 2\pi. \tag{A.2}$$

As seen, when the angle $\phi = 0$, there is $q_+ = [1, 0, 0, 0]$, and when $\phi = 2\pi$, correspondingly $q_- = [-1, 0, 0, 0]$. Because of $\ln q_+ = \ln q_- = (0, 0, 0)$, it is obvious that a unit quaternion can be transformed to a three-dimensional vector by the logarithm operation.

The definition of dual numbers is

$$\widehat{a} = a + \varepsilon a', \tag{A.3}$$

where a and a' are, respectively, called real part and dual part. ε is called the dual unit, satisfying $\varepsilon^2 = 0$ and $\varepsilon \neq 0$. And the operation of the dual numbers is defined as

$$\begin{aligned} \widehat{a}_1 + \widehat{a}_2 &= a_1 + a_2 + \varepsilon\left(a_1' + a_2'\right); \\ \lambda\widehat{a} &= \lambda a + \varepsilon\lambda a', \\ \widehat{a}_1\widehat{a}_2 &= a_1 a_2 + \varepsilon\left(a_2 a_1' + a_1 a_2'\right), \end{aligned} \tag{A.4}$$

where λ is a scalar.

The dual vector is that both the dual part and real part are vectors. For two dual vectors $\widehat{v}_1 = v_1 + \varepsilon v_1'$ and $\widehat{v}_2 = v_2 + \varepsilon v_2'$, their cross multiplication is

$$\begin{aligned} \widehat{v}_1 \times \widehat{v}_2 &= v_1 \times v_2 + \varepsilon\left(v_1 \times v_2' + v_1' \times v_2\right), \\ \langle \widehat{v}_1, \widehat{v}_2 \rangle &= v_1^{\mathrm{T}} v_1' + v_2^{\mathrm{T}} v_2'. \end{aligned} \tag{A.5}$$

In addition to this, dual number $\widehat{a}$ and dual vector $\widehat{v}$ have the following operation:

$$\widehat{a} \odot \widehat{v} = av + \varepsilon a' v'. \tag{A.6}$$

Data Availability

The data used to support the findings of this study are available from the corresponding author upon request.

Conflicts of Interest

The authors declare that they have no conflicts of interest.

Acknowledgments

This work was supported by the Major Program of National Natural Science Foundation of China under Grant nos. 61690210 and 61690213.

References

[1] A. E. White and H. G. Lewis, "The many futures of active debris removal," *Acta Astronautica*, vol. 95, pp. 189–197, 2014.

[2] R. A. Gangapersaud, G. Liu, and A. H. J. De Ruiter, "Detumbling of a non-cooperative target with unknown inertial parameters using a space robot," *Advances in Space Research*, vol. 63, no. 12, pp. 3900–3915, 2019.

[3] B. W. Barbee, J. R. Carpenter, S. Heatwole et al., "A guidance and navigation strategy for rendezvous and proximity operations with a noncooperative spacecraft in geosynchronous orbit," *The Journal of the Astronautical Sciences*, vol. 58, no. 3, pp. 389–408, 2011.

[4] N. FitzCoy and M. Liu, "Modified proportional navigation scheme for rendezvous and docking with tumbling targets: the planar case," in *Proceedings of the Symposium on Flight Mechanics/Estimation Theory*, pp. 243–252, Greenbelt, MD, USA, May 1995.

[5] S. Nakasuka and T. Fujiwara, "New method of capturing tumbling object in space and its control aspects," in *Proceedings of the presented at the IEEE International Conference on Control Applications*, Kohala Coast, HI, USA, August 1999.

[6] Y. Tsuda and S. Nakasuka, "New attitude motion following control algorithm for capturing tumbling object in space," *Acta Astronautica*, vol. 53, no. 11, pp. 847–861, 2003.

[7] G. Boyarko, O. Yakimenko, and M. Romano, "Optimal rendezvous trajectories of a controlled spacecraft and a tumbling object," *Journal of Guidance, Control, and Dynamics*, vol. 34, no. 4, pp. 1239–1252, 2011.

[8] W. Fehse, *Automated Rendezvous and Docking of Spacecraft: The Drivers for the Approach Strategy*, pp. 8–74, Cambridge University Press, London, UK, 2003.

[9] Z. Ma, O. Ma, and B. Shashikanth, "Optimal control for spacecraft to rendezvous with a tumbling satellite in a close range," in *Proceedings of the presented at the 2006 IEEE/RSJ International Conference on Intelligent Robots and Systems*, Beijing, China, October 2006.

[10] M. Wilde, M. Ciarcià, A. Grompone, and M. Romano, "Experimental characterization of inverse dynamics guidance in docking with a rotating target," *Journal of Guidance, Control, and Dynamics*, vol. 39, no. 6, pp. 1173–1187, 2016.

[11] Z. Xu, X. Chen, Y. Huang, Y. Bai, and W. Yao, "Nonlinear suboptimal tracking control of spacecraft approaching a tumbling target," *Chinese Physics B*, vol. 27, no. 9, Article ID 090501, 2018.

[12] J. Wang, H. Liang, Z. Sun, S. Zhang, and M. Liu, "Finite-time control for spacecraft formation with dual-number-based description," *Journal of Guidance, Control, and Dynamics*, vol. 35, no. 3, pp. 950–962, 2012.

[13] I. S. Fisher, *Dual-Number Methods in Kinetics, Statics and Dynamics*, p. 66, CRC Press, Boca Raton, FL, USA, 1999.

[14] A. T. Yang, *Application of Quaternion Algebra and Dual Numbers to the Analysis of Spital Mechanisms*, Columbia University, New York, NY, USA, 1964.

[15] V. Brodsky and M. Shoham, "Dual numbers representation of rigid body dynamics," *Mechanism and Machine Theory*, vol. 34, no. 5, pp. 693–718, 1999.

[16] J. Wu, D. Han, K. Liu, and J. Xiang, "Nonlinear suboptimal synchronized control for relative position and relative attitude tracking of spacecraft formation flying," *Journal of The Franklin Institute*, vol. 352, no. 4, pp. 1495–1520, 2015.

[17] J. Wu, K. Liu, and D. Han, "Adaptive sliding mode control for six-DOF relative motion of spacecraft with input constraint," *Acta Astronautica*, vol. 87, pp. 64–76, 2013.

[18] N. Filipe and P. Tsiotras, "Adaptive position and attitude-tracking controller for satellite proximity operations using dual quaternions," *Journal of Guidance, Control, and Dynamics*, vol. 38, no. 4, pp. 566–577, 2015.

[19] H. Dong, Q. Hu, and M. R. Akella, "Dual-quaternion-based spacecraft autonomous rendezvous and docking under six-degree-of-freedom motion constraints," *Journal of Guidance, Control, and Dynamics*, vol. 41, no. 5, pp. 1150–1162, 2018.

[20] G. A. Jr. and L. S. Martins-Filho, "Guidance and control of position and attitude for rendezvous and dock/berthing with a noncooperative/target spacecraft," *Mathematical Problems in Engineering*, vol. 2014, Article ID 508516, 8 pages, 2014.

[21] Q. Ni, Y. Huang, and X. Chen, "Nonlinear control of spacecraft formation flying with disturbance rejection and collision avoidance," *Chinese Physics B*, vol. 26, no. 1, Article ID 014502, 2017.

[22] P. Razzaghi, E. Al Khatib, and S. Bakhtiari, "Sliding mode and SDRE control laws on a tethered satellite system to de-orbit space debris," *Advances in Space Research*, vol. 64, no. 1, pp. 18–27, 2019.

[23] J. Wang and Z. Sun, "6-DOF robust adaptive terminal sliding mode control for spacecraft formation flying," *Acta Astronautica*, vol. 73, pp. 76–87, 2012.

[24] A.-M. Zou, K. D. Kumar, Z.-G. Hou, and L. Xi, "Finite-time attitude tracking control for spacecraft using terminal sliding mode and Chebyshev neural network," *IEEE Transactions on Systems Man and Cybernetics Part B-(Cybernetics)*, vol. 41, no. 4, pp. 950–963, 2011.

[25] J. A. Moreno and M. Osorio, "A Lyapunov approach to second-order sliding mode controllers and observers," in *Proceedings of the 47th IEEE Conference on Decision and Control*, vol. 16, no. 5, pp. 2856–2861, Cancun, Mexico, December 2008.

[26] S. Wu, R. Wang, G. Radice, and Z. Wu, "Robust attitude maneuver control of spacecraft with reaction wheel low-speed friction compensation," *Aerospace Science and Technology*, vol. 43, pp. 213–218, 2015.

[27] R. Yan and Z. Wu, "Nonlinear disturbance observer based spacecraft attitude control subject to disturbances and actuator faults," in *Proceedings of the American Institute of Physics Conference Series*, vol. 1834, no. 1, Athens, Greece, April 2017.

[28] C. Pukdeboon, "Extended state observer-based third-order sliding mode finite-time attitude tracking controller for rigid spacecraft," *Science China Information Sciences*, vol. 62, no. 1, pp. 1–16, 2019.

[29] Y. Xia, Z. Zhu, M. Fu, and S. Wang, "Attitude tracking of rigid spacecraft with bounded disturbances," *IEEE Transactions on Industrial Electronics*, vol. 58, no. 2, pp. 647–659, 2011.

[30] X. Huang, Y. Yan, and Y. Zhou, "Nonlinear control of underactuated spacecraft hovering," *Journal of Guidance, Control, and Dynamics*, vol. 39, no. 3, pp. 685–694, 2015.

[31] L. Zhang, C. Wei, R. Wu, and N. Cui, "Fixed-time extended state observer based non-singular fast terminal sliding mode control for a VTVL reusable launch vehicle," *Aerospace Science and Technology*, vol. 82-83, pp. 70–79, 2018.

[32] D. Ran, X. Chen, A. de Ruiter, and B. Xiao, "Adaptive extended-state observer-based fault tolerant attitude control for spacecraft with reaction wheels," *Acta Astronautica*, vol. 145, pp. 501–514, 2018.

[33] J. Zhang, D. Ye, Z. Sun, and C. Liu, "Extended state observer based robust adaptive control on SE(3) for coupled spacecraft tracking maneuver with actuator saturation and misalignment," *Acta Astronautica*, vol. 143, pp. 221–233, 2018.

[34] E. Jin and Z. Sun, "Robust controllers design with finite time convergence for rigid spacecraft attitude tracking control," *Aerospace Science and Technology*, vol. 12, no. 4, pp. 324–330, 2008.

[35] S. Yu, X. Yu, B. Shirinzadeh, and Z. Man, "Continuous finite-time control for robotic manipulators with terminal sliding mode," *Automatica*, vol. 41, no. 11, pp. 1957–1964, 2005.

[36] H. D. He, D. Y. Wang, and H. Gao, "Vision-based position and pose determination of non-cooperative target for on-orbit servicing," *Multimedia Tools and Applications*, pp. 1–14, 2018.

[37] L. Wang, T. Chai, and L. Zhai, "Neural-network-based terminal sliding mode control of robotic manipulators including actuator dynamics," *IEEE Transactions on Industrial Electronics*, vol. 56, no. 9, pp. 3296–3304, 2009.

[38] Y. Feng, X. Yu, and Z. Man, "Non-singular terminal sliding mode control of rigid manipulators," *Automatica*, vol. 38, no. 12, pp. 2159–2167, 2002.

[39] X. Huang, Y. Yan, and Z. Huang, "Finite-time control of underactuated spacecraft hovering," *Control Engineering Practice*, vol. 68, pp. 46–62, 2017.